



# Cardiac CT perfusion and $FFR_{CTA}$ : pathophysiological features in ischemic heart disease

Sara Seitun<sup>1</sup>, Alberto Clemente<sup>2</sup>, Cecilia De Lorenzi<sup>1</sup>, Stefano Benenati<sup>3</sup>, Dante Chiappino<sup>2</sup>, Cesare Mantini<sup>4</sup>, Antonis I. Sakellarios<sup>5</sup>, Filippo Cademartiri<sup>6</sup>, Gian Paolo Bezante<sup>3</sup>, Italo Porto<sup>3</sup>

<sup>1</sup>Department of Radiology, IRCCS Policlinico San Martino Hospital, Genoa, Italy; <sup>2</sup>Department of Radiology, CNR (National Council of Research)/Tuscany Region ‘Gabriele Monasterio’ Foundation (FTGM), Massa, Italy; <sup>3</sup>Clinic of Cardiovascular Diseases, IRCCS Policlinico San Martino Hospital, University of Genoa, Genoa, Italy; <sup>4</sup>Department of Neuroscience, Imaging and Clinical Science, Institute of Radiology, ‘G. d’Annunzio’ University, Chieti, Italy; <sup>5</sup>Unit of Medical Technology and Intelligent Information Systems, Department of Materials Science and Engineering, University of Ioannina, Ioannina, Greece; <sup>6</sup>SDN IRCCS, Naples, Italy

**Contributions:** (I) Conception and design: S Seitun, F Cademartiri; (II) Administrative support: S Seitun, A Clemente, F Cademartiri, GP Bezante; (III) Provision of study materials or patients: S Seitun, A Clemente, C De Lorenzi, AI Sakellarios, S Benenati; (IV) Collection and assembly of data: All authors; (V) Data analysis and interpretation: All authors; (VI) Manuscript writing: All authors; (VII) Final approval of manuscript: All authors.

**Correspondence to:** Dr. Alberto Clemente, MD. Department of Radiology, CNR (National Council of Research)/Tuscany Region ‘Gabriele Monasterio’ Foundation (FTGM), Via Aurelia Sud, Massa 54100, Italy. Email: alberto.clemente@ftgm.it.

**Abstract:** Cardiac computed tomography (CCT) has rapidly evolved, becoming a powerful integrated tool for the evaluation of coronary artery disease (CAD), and being superior to other noninvasive methods due to its high accuracy and ability to simultaneously assess both lumen stenosis and atherosclerotic plaque burden. Furthermore, CCT is regarded as an effective gatekeeper for coronary angiography, and carries independent important prognostic information. In the last decade, the introduction of new functional CCT applications, namely CCT perfusion (CCTP) imaging and CT-derived fractional flow reserve ( $FFR_{CTA}$ ), has opened the door for accurate assessment of the haemodynamic significance of stenoses. These new CCT technologies, thus, share the unique advantage of assessing both myocardial ischemia and patient-specific coronary artery anatomy, providing an integrated anatomical/functional analysis. In the present review, starting from the pathophysiology of myocardial ischemia, we evaluate the existing evidence for functional CCT imaging and its value in relation to alternative, well-established, non-invasive imaging modalities and invasive indices of ischemia (currently the gold-standard). The knowledge of clinical applications, benefits, and limitations of these new CCT technologies will allow efficient and optimal use in clinical practice in the near future.

**Keywords:** Cardiac computed tomography (CCT); cardiac CT perfusion; fractional flow reserve (FFR);  $FFR_{CTA}$ ; computational fluid dynamics (CFD)

Submitted Apr 02, 2020. Accepted for publication Apr 22, 2020.

doi: 10.21037/cdt-20-414

**View this article at:** <http://dx.doi.org/10.21037/cdt-20-414>

## Introduction

Cardiac computed tomography (CCT) has undergone an exponential growth during the last two decades, from the first multi-detector CT scanners up to the latest machines characterized by significantly higher contrast, temporal and spatial resolution. CCT role in the cardiovascular field is unchallenged in specific settings,

such as measuring coronary artery calcium score (CACS) in the intermediate-risk asymptomatic subjects (1), CT coronary angiography (CTCA) in symptomatic patients with low-to-intermediate pretest probability of coronary artery disease (CAD) (2-5) or in patients with acute chest pain and low [0 to 2] Thrombolysis in Myocardial Infarction (TIMI) risk score (6),

and CTCA for pre-procedural planning of structural heart disease (7). In particular, in the setting of ischemic heart disease, CTCA has shown high sensitivity and very high negative predictive value ( $\geq 95\%$ ) for significant CAD (8,9). CTCA also carries an important prognostic value, being the only technique able to measure atheroma burden along the entire length of the coronary arteries (10-14) and assess its composition (15). The large multi-center SCOT-HEART (16) and PROMISE (17) trials have supported a role for CTCA in diagnosis of significant CAD in stable patients, due to a significantly lower rates of mortality from CAD and nonfatal myocardial infarction in the CTCA arm as compared to standard care (16) or functional testing (17). Furthermore, in the 5-year follow-up of the SCOT-HEART, CTCA, in addition to standard care in patients with stable chest pain, resulted in lower cardiovascular death without an increase in coronary angiography (CA) or revascularization (18). In consideration of this strong evidence, latest European guidelines for the diagnosis and management of chronic coronary syndromes recommend CTCA as first tool to rule out CAD in patients in whom ischemic disease cannot be excluded by clinical assessment alone (class I LoE B) (19).

Despite CTCA being useful to detect coronary lumen stenoses, its main limitation relies on the impossibility to assess their functional significance, especially in the intermediate range (40–80%), a consequence of its, at best, moderate positive predictive value (about 50%) (20). In contrast, other non-invasive techniques such as stress echocardiography, stress single-photon emission computed tomography (SPECT), stress cardiac magnetic resonance imaging (MRI) and positron emission tomography (PET) are better suited to evaluate myocardial perfusion and/or ischemia, but provide limited information regarding anatomy (21-23). Thus, none of these techniques is able to provide a comprehensive anatomical-functional assessment of a coronary stenosis-inducing plaque within the same study. Of note, current practice guidelines support the clinical benefit of ischemia-guided selective revascularization based on non-invasive and invasive functional evaluation, which reduces the risk of major acute cardiovascular events including myocardial infarction and cardiovascular death (19,24).

In the last decade, rapid technological improvements of CCT technology resulting in reduction of the scan time, motion artefacts and radiation dose exposure, while yielding higher spatial and temporal resolution (25-27), have widened CCT field of application, from anatomical detection of CAD

to physiological assessment of myocardial ischemia. The first human report of stress myocardial CCT perfusion (CCTP) by Kurata *et al.* was published in 2005 with a 16-slice CT scanner and using adenosine triphosphate stress (28). Currently, feasibility of CCTP imaging with modern multi-detector row ( $\geq 64$  slices) CT systems at rest and during pharmacologic stress has been demonstrated by clinical studies and recent multicenter trials (29-40). Moreover, by applying principle of computational fluid dynamics (CFD) algorithms, a non-invasive approximation of fractional flow reserve (FFR) from resting CTCA dataset ( $FFR_{CTA}$ ) may be derived to assess lesion-specific ischemia and guide revascularization (33).

The purpose of this narrative review is to describe the principles, clinical applications, and current state of the art of these new CCT technologies, comparing them with FFR and non-invasive techniques.

## Myocardial ischemia

### *Pathophysiology of myocardial ischemia*

The term myocardial ischemia refers to an imbalance between myocardial oxygen demand and supply. Myocardial oxygen consumption ( $MVO_2$ ) is determined by fixed (myocardial mass) and modifiable (heart rate, systemic blood pressure, wall stress in terms of pre- and post-load and inotropic status) parameters. Heart rate is the main  $MVO_2$  influencing factor, as an increase in contraction velocity needs an increase of oxygen delivery. Wall stress is influenced by pre-load, which is the diastolic blood volume linked to venous return, and post-load, which is the tension that myocardial muscle needs to develop for starting and maintaining systolic ejection. The latter can be approximated with systemic arterial pressure, which represents the second determinant of  $MVO_2$  in the order of importance. In clinical practice a good approximation of  $MVO_2$  can be obtained by calculating the so-called “double-product” (systolic pressure x heart rate). Inotropic status refers to the strength of myocardial contraction and has a more complex relation to  $MVO_2$  because of adaptive mechanisms and neurohormonal state; according to Frank-Starling law, within physiological limits, an increase in diastolic volume (pre-load) is associated with an increase in the force of contraction (41).

Myocardial oxygen delivery depends upon oxygen blood concentration and coronary blood flow. Oxygen carriage by the blood can be disrupted by a fall in haemoglobin

(anemia) or by a reduced oxygen binding capacity. In basal conditions, O<sub>2</sub> extraction by myocytes is very high (around 70%); thus, the only mechanism to increase O<sub>2</sub> delivery is a proportional augmentation in blood supply. In normal haemodynamic conditions, coronary auto-regulation (the ability of coronary arteries to keep blood flow constant over a wide reduction in aortic pressure) allows to maintain normal regional perfusion if determinants of myocardial oxygen consumption do not change (42). This is due to vasodilation in response to intrinsic factors (local metabolites, endothelial factors and neural tone) or extrinsic stimulation (i.e., adenosine).

The ability to increase flow above resting values is termed coronary flow reserve (CFR). When pressure falls beyond the lower limit of auto-regulation, coronary resistance vessels are maximally vasodilated due to intrinsic stimuli, and flow becomes pressure-dependent, resulting in the onset of sub-endocardial ischemia (42,43).

### *Causes of myocardial ischemia*

The main cause of myocardial ischemia is coronary atherosclerosis, which leads to artery wall thickening and atheroma accumulation in epicardial vessels with reduction in its lumen diameter. Due to coronary autoregulation, myocardial perfusion at rest is generally normal until the luminal diameter narrowing exceeds 85–90%. However, stenosis >50% in condition of increased O<sub>2</sub> requirement, i.e., physical exertion, can induce a reduction in CFR, leading to tissue ischemia (23,44). This physiological phenomenon is the basis of the stress tests commonly used to diagnose myocardial ischemia. Other possible causes of ischemia are microvascular disease (which escape the resolution of angiographic techniques) and vasospastic angina; they are typically associated with either no stenoses or mild-to-moderate stenoses that are deemed functionally non-relevant (19).

Although ischemia is often indicative of a coronary artery stenosis, this cause-effect relationship is not perfect. In fact, some severe stenotic lesions do not produce significant ischemia, whereas other mild/moderate stenosis may cause both ischemia and cardiac events (19).

This poor correlation has been reassessed in a sub-study of the FAME (Fractional Flow Reserve Versus Angiography in Multivessel Evaluation) trial, which assessed 1,329 lesions by FFR in 509 patients with multivessel CAD. In stenoses categorized as 50–70% by visual angiographic assessment, 35% of the cases were functionally significant (FFR ≤0.80)

and 65% were not (FFR >0.80). Among stenoses categorized as 71–90%, 80% were functionally significant (FFR ≤0.80) and 20% were not (FFR >0.80). In the category of subtotal stenoses (91–99%), only 4% of the cases were not significant (FFR was >0.8), and the remaining 96% were functionally significant stenoses (FFR ≤0.80) (45).

### *Ischemia detection*

Non-invasive imaging is essential in the diagnosis and management of ischemic heart disease from its earliest manifestations of endothelial dysfunction to myocardial infarction (46). The preferred method to induce ischemia is physical exercise, albeit pharmacological stress agents can be used with similar (but by no means identical) accuracy. Drugs frequently employed are adenosine, dipyridamole, dobutamine or regadenoson. Adenosine provides a nonselective activation of four distinct subtypes (A1, A2A, A2B, and A3) receptors. Compared to dipyridamole, adenosine has a more rapid onset of action and a shorter half-life (around 30 s); therefore, most side effects resolve in a few seconds after discontinuation of the adenosine infusion. Side effects could be AV block, peripheral vasodilation, and bronchospasm, but the most common are flushing, chest pain, dyspnea, dizziness, or nausea.

Dipyridamole inhibits cellular uptake of adenosine, indirectly leading to coronary arteriolar vasodilation. Due to its longer half-life of approximately 30 minutes, patients given this drug may require administration of aminophylline for reversal of persistent symptoms (33,47).

The synthetic catecholamine dobutamine is primarily a β<sub>1</sub>-adrenergic receptors agonist, with mild effect on α<sub>1</sub>- and β<sub>2</sub>-receptors. At low doses (≤10 μg/kg/min), dobutamine improves myocardial contractility and induces coronary vasodilation; at higher doses (20–40 μg/kg/min), it causes systemic vasodilation and exerts a positive chronotrope effect (48). Dobutamine is used for stress echocardiography or stress MRI to detect myocardial ischemia by identifying regional wall motion abnormalities (RWMA), with accuracy and sensitivity similar to dipyridamole-stress imaging (48).

Finally, regadenoson, an A<sub>2A</sub> selective agonist has been recently introduced as a vasodilator. It has a safer side effect profile in comparison to adenosine and dipyridamole, especially for patients with asthma or severe chronic obstructive pulmonary disease. Its use is mainly limited by cost and it is also not widely available. Regadenoson has been shown to be accurate for the detection of obstructive CAD in nuclear perfusion imaging, stress echocardiography,

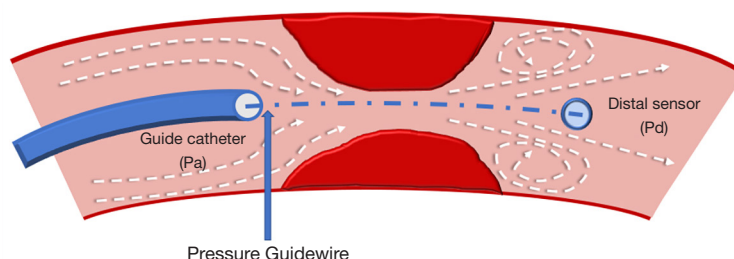


**Figure 1** Invasive fractional flow reserve (FFR) in the catheter laboratory to guide revascularization. Concomitant measurement of aortic pressure (Pa) with a guide catheter and distal coronary pressure (Pd) with the pressure guidewire across a coronary stenosis performed during maximal hyperaemia.

and, more recently, stress CCTP studies (49,50).

### Haemodynamic significance of coronary stenosis: evaluation in the catheterization laboratory

Numerous invasive physiological indices of ischemia have been developed in the last two decades, with the aim of overcoming the obvious limitations of CA (in effect, a bidimensional “luminogram”) in guiding percutaneous coronary intervention (PCI) (51).

The pathophysiological assumption is that, during maximal hyperaemia, when arteriolar regulation is blunted, the flow across a stenosis exclusively hinges on the pressure gradient. In this scenario, the pressure drop from the upstream to the downstream portion of the vessel linearly approximates blood flow reduction attributable to the stenosis, unveiling its ischemic potential (52).

FFR was hence defined as the ratio between the pressure measured distally from a given stenosis (Pd) and that achieved in the proximal part of the vessel (Pa) under maximal hyperaemia, with the latter obtained through a transient pharmacological stimulus (e.g., intravenous adenosine) (*Figure 1*). Of note, being a ratio of two pressures, FFR is a dimensionless number.

The accepted FFR value to detect haemodynamically relevant stenoses has been initially set to 0.75 (e.g., a 25% reduction in the maximum achievable flow induced by the stenosis), under which revascularization was recommended in the initial physiology-guided PCI trials (52). However, the so-called “grey zone” ranging from 0.75–0.80 has been subsequently included in the FFR values prompting revascularization (52), mainly due to the appreciation that FFR values distribution is effectively a spectrum, with no clear cut-off.

Randomized clinical trials (RCTs) supported the superiority of FFR compared to standard CA in guiding PCI of angiographically intermediate lesions of both stable patients (53) and non-infarct related arteries of acute coronary syndromes (54). The use of FFR was shown to modify the treatment strategy (medical therapy, PCI or coronary bypass graft) in one out of four patients (55). Yet, real-life data point out a linear relationship between FFR values and cardiovascular events (56). On the other hand, concerns have arisen on the reliability of FFR in certain clinical settings (e.g., aortic stenosis or chronic total occlusion) (57) and the safety and tolerability of vasodilators (58). Moreover, it is a rather expensive procedure (around 1,000 USD) (59). These factors have prompted the search for further non-hyperaemia dependent or “resting” indices of ischemia.

During the cardiac cycle, microvascular resistance sways, mirroring the alternation between systolic squeezing and diastolic relaxation and causing a succession of compression and suction waves, which propagate from the proximal (aortic) and distal (microcirculatory) parts of the vessel. Wave-intensity analysis allows the identification of a specific time-frame, occurring during diastole, in which no further waves are generated. In this “wave-free period” (WFP) microvascular resistance drops and becomes constant (as after maximal pharmacological vasodilation), and the distal to proximal pressure ratio across a stenosis provides an instantaneous wave-free ratio (iFR), potentially enabling the assessment of ischemia at rest and tightly correlating with FFR (60). In fact, according to two recent large-scale RCTs, iFR was non-inferior compared to FFR, showing moreover a reduction of patient’s discomfort and procedure length (61,62). Both these studies used an iFR cut-off at 0.89, which matches with an FFR ischemic cut-point of 0.80 (62) (*Figure 2*).

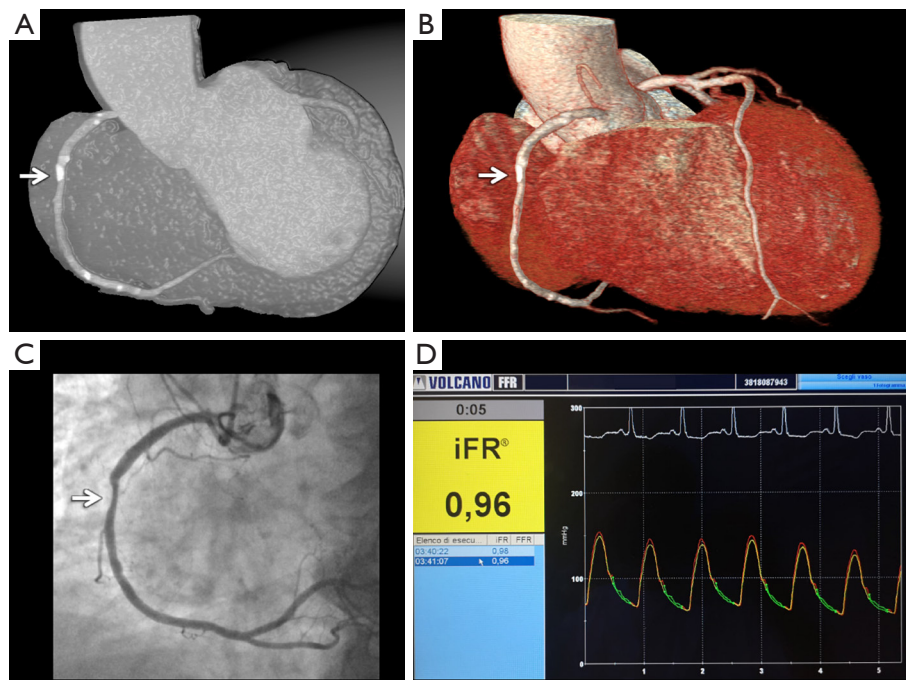


**Figure 2** An 87-year-old female with multiple cardiovascular risk factors (obesity, arterial hypertension, past smoking, chronic obstructive pulmonary disease) presented with atypical chest pain and exertional dyspnea. 3D maximum intensity projection (MIP, A) and volume rendering technique (VRT, B) coronary CT angiography reconstructions show a calcified eccentric plaque causing a sub-critical stenosis (approximately 60%) at the middle segment of the right coronary artery (RCA). Invasive coronary angiography (C) confirms the coronary stenosis (arrow). (D) The instantaneous wave-free ratio (iFR) result demonstrates a measurement of 0.96, which is above its cut-off value of 0.89. Thus, the stenosis is classified as not hemodynamically relevant, and consequently would not benefit from revascularization.

More recently, further attempts have been made in search of quicker, safer and equally performing invasive indices. For instance, unlike iFR, the resting full-cycle ratio (RFR) measures the lowest distal to proximal pressure ratio (Pd/Pa) during the entire coronary cycle (63), whereas the diastolic pressure ratio (dPR) is the average diastolic (not restricted to the WFP) Pd/Pa (64). Both of them showed a high agreement with iFR and FFR and were correlated with the risk of vessel-oriented outcomes (65).

Finally, advances in CFD have laid the foundation for angiography-based indices. In a nutshell, these are based on a three-dimensional reconstruction of the coronary tree and calculated by specific software using CFD algorithms. Among them, quantitative flow ratio (QFR) derives from single-vessel 3D-reconstructions and utilizes TIMI frame count as a surrogate of blood flow (66), whereas coronary angiography-derived FFR (FFRangio) is based on a three-vessel reconstruction and subsequent estimation of resistance and flow through scaling-laws (67).

### Cardiac CT perfusion: technical prerequisites and imaging protocols

The first attempts of myocardial perfusion analysis by CCT date back to the late 1970's and early 1980's, with experimental animal studies in infarct imaging which demonstrated the potential of the early generation head CT scanners to delineate differences in contrast media attenuation between normal and infarcted myocardium of various ages (68,69). During the last decade, important technical developments have rediscovered multi-slice CCT for cardiac perfusion imaging, transforming CCT from purely anatomical analysis of coronary stenosis and atherosclerotic plaques to functional myocardial perfusion analysis. Ongoing advances in scanner technology include higher temporal resolution (up to 66 ms with third generation dual-source CT scanner), higher spatial resolution (due to increase in detector sensitivity and efficiency), improved scan speed, wider detectors array (with a z-axis coverage as high as 16 cm with the 320-slice

**Table 1** Major advantages and limitations of stress/rest and rest/stress protocols for myocardial perfusion imaging

Protocol	Advantages	Limitations
Rest/stress	More suitable in patients at low-to-intermediate pre-test probability of obstructive CAD	Risk of cross-contamination of contrast in the stress phase—less sensitivity for the detection of inducible myocardial perfusion defects
	A “normal” coronary rest scan with absence of obstructive CAD does not require subsequent stress scan—“rest only” protocol with reductions in the radiation and contrast medium doses	Beta-blocker administered before the stress acquisition may lead to underestimation of myocardial ischemia
	High sensitivity for the detection of myocardial necrosis	
Stress/rest	More suitable in patients with high pre-test probability of obstructive CAD, extensive calcifications, previous revascularization (multiple stents) or known multi-vessel CAD	Risk of imaging quality degradation of rest phase caused by persistent high heart rate response to long half-life vasodilator stress agents
	High sensitivity for the detection of ischemia without the risk of cross-contamination of contrast from the rest phase	Less sensitivity for the detection of fixed perfusion defect (infarction) in the rest phase because of relative hyper-enhancement of scar
	Absence of interference of beta-blockers or nitrates administered for coronary anatomy evaluation	The stress scan is performed without the knowledge of the presence of obstructive CAD

CAD, coronary artery disease.

CT system), and improved image quality due to advanced iterative reconstruction algorithms (23). Currently, a 64 slices CT scanner is considered the minimum technology requirement that meets the basic needs for CCTP imaging (23).

CCTP is performed in a similar way to other imaging perfusion techniques, such as stress SPECT or MRI, by means of rest and stress imaging acquisitions during continuous monitoring of heart rate, blood pressure, and ECG. A comprehensive CCTP protocol typically involves: (I) a rest scan, which is used to evaluate both coronary stenosis and myocardial perfusion at rest, (II) a stress scan during administration of intravenous vasodilator drugs (e.g., adenosine, dipyridamole or regadenoson) to assess inducible myocardial perfusion defects, (III) an optional late-enhancement scan recommended in selected cases performed approximately 5–10 minutes after the last contrast injection, which is used to assess myocardial viability (34). A stress-first or rest-first protocols have been reported, with its own advantages and disadvantages (Table 1).

Two main techniques for pharmacological stress CCTP imaging have been developed: the *static* and the *dynamic* CCTP scan acquisitions.

### *Static cardiac CT perfusion imaging*

The *static* CCTP acquisition, using single-energy or dual-

and multi-energy techniques, relies on the acquisition of a single imaging dataset during the first-pass of contrast media thorough the myocardium providing a snapshot of myocardial enhancement (iodine distribution) at one stationary time point (23). Therefore, the timing of the scan acquisition needs to be carefully optimized in relation to the injection protocol, in order to acquire the images at the highest contrast-to-noise ratio difference between the normal and ischemic myocardium (23). Interpretation of static CCTP imaging is based on qualitative visual analysis of differences in contrast attenuation within the myocardium. Similar to nuclear imaging, “reversible” subendocardial and transmural perfusion defects are consistent with inducible myocardial ischemia, whereas “fixed” hypo-attenuated defects seen at both rest and stress phases suggest scar tissue, i.e., a myocardial infarct (34). The presence of other signs of myocardial necrosis/fibrosis (myocardial thinning; calcifications; lipomatous metaplasia; aneurysmal/pseudoaneurysmal dilation; mural thrombus; or wall motion abnormalities) on rest imaging further confirms prior infarct (34). Finally, automated software applications providing 3D modelling and 17-segment bull’s-eye plot of the left ventricular perfusion are available (23) (Figure 3).

Dual- or multi-energy CT consists in image acquisition at different energy levels with several technical approaches by various vendors, which include dual X-ray sources working at two different energy level (70–80–90/140–150 kVp),

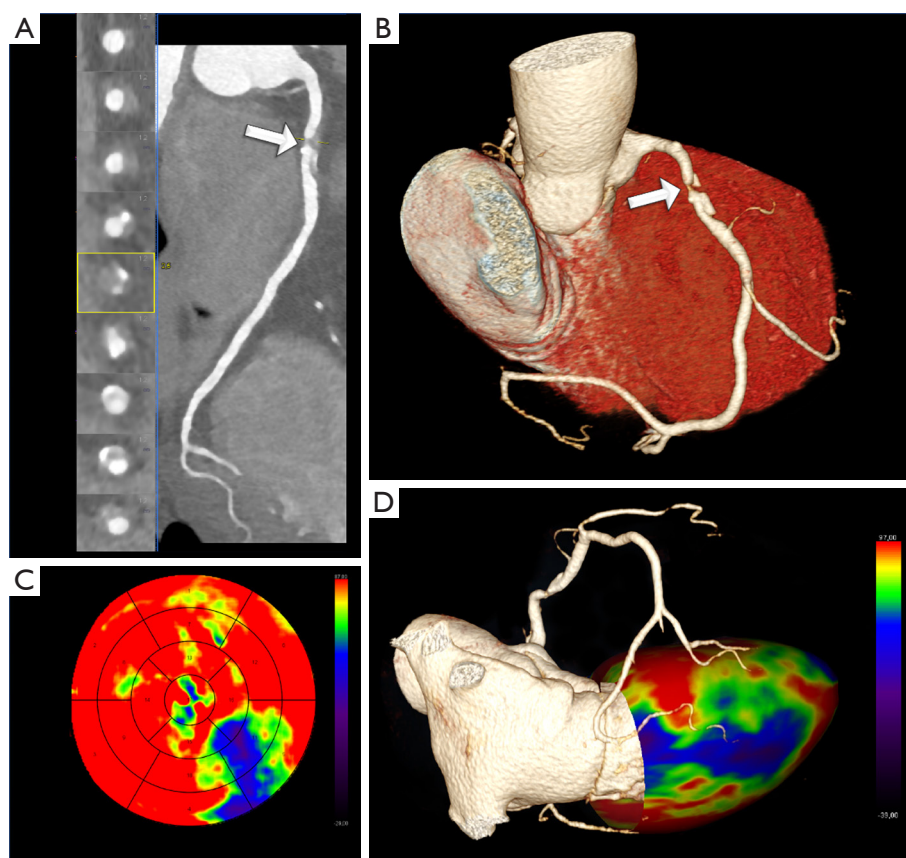


**Figure 3** Static CT myocardial perfusion imaging. A 67-year-old male patient presented with typical chest pain and exertional dyspnea. Curved multiplanar (A) and 3D volume rendering technique (VRT, B) coronary CT angiography reconstructions show a mixed atherosclerotic plaque with positive remodeling causing a critical stenosis (>70% luminal narrowing) at the proximal segment of the right coronary artery (RCA) (arrows). A 17-segment polar plot (C) and volume rendering reconstruction with overimposed myocardial blood flow map and coronary tree (D), acquired with a prospectively ECG triggered high-pitch spiral technique at stress during the first pass, arterial phase, showed the presence of extensive perfusion defects of the inferior and inferolateral walls, color-coded in blue/green.

two sequential scans (not used for cardiac imaging), rapid switching (less than 1 ms) between the low- and high-energy of X-ray tube potential, and multilayer detector. Dual- or multi-energy CCTP enables differentiation by analyzing material-dependent photo-electric effect and Compton scattering processes (35,70). Dual- or multi-energy CCTP imaging may offer some advantages over single-energy CCTP by identification of iodine voxels within the myocardium, providing an estimate of contrast distribution across the myocardium at one point in time. Dual- or multi-energy CCTP allows accurate iodine quantification and distribution, which has a direct relation to myocardial blood flow (MBF), and thus provides a semi-quantitative marker of myocardial perfusion (35,71). Dual- or multi-energy datasets are post-processed using dedicated

vendor-specific softwares which generate color-coded maps (iodine material density images) highlighting myocardial perfusion defects or late-enhancement of iodinated areas.

#### *Dynamic cardiac CT perfusion imaging*

Unlike static CCTP scan, *dynamic* CCTP imaging allows the acquisition of several imaging dataset at multiple time-points following contrast injections during a 20–30 seconds inspiratory breath-hold. Currently, there are two CT scanner techniques that enable dynamic CCTP, the prospective ECG-gated dynamic acquisition mode with a large coverage CT scanner along the z-axis (256- or 320-detector-row CT scanners) or, in the case of narrow detectors, the ECG-triggered axial shuttle mode technique

implemented with the second- and third-generation dual-source CT scanners.

A high flow rate of injection of contrast media (at least 5 mL/s) is indicated to ensure a compact bolus and accurately defines arterial and myocardial peak enhancement for modelling. The multi-phasic dataset is used to generate time-attenuation curves (TACs) for each voxel of left ventricular myocardium and the reference arterial input function (AIF, derived from the left ventricle or the thoracic aorta). Using a dedicated parametric deconvolution based on 2-compartment model of intra- and extravascular space to fit the TACs, dynamic CCTP imaging enables absolute quantification of myocardial perfusion haemodynamic parameters such as MBF (mL/100 mL/min), MBF ratio, and myocardial blood volume (MBV, mL/100 mL) according to the formulas:  $MBF = \text{MaxSlope}(\text{TissueTAC}) / \text{Maximum}(\text{AIF})$ ;  $MBV = \text{Maximum}(\text{TissueTAC}) / \text{Maximum}(\text{AIF})$  (23,33). Furthermore, semi-quantitative parameters such as the peak enhancement, time to peak (TTP), up-slope, tissue transit time (TTT), and area under the curve (AUC) are derived (in a similar manner than for semi-quantitative dynamic MRI perfusion imaging). Finally, by comparing MBF during stress and rest phases, an assessment of absolute CFR may be obtained (72).

Similar to visual dynamic MRI, time-resolved CCTP acquisition may be evaluated for relative areas of hypo-perfusion over time (34). Further post-processing analysis of dynamic CCTP images are based on fully automatic and semiautomatic method with generation of color-coded polar maps and overlay images for each perfusion parameter (73,74) (Figure 4).

Major differences between the static and the dynamic CCTP imaging are reported in Table 2.

### *Accuracy of cardiac CT perfusion*

At present, various single-center experiences and first multi-center trials have evaluated the diagnostic performance of CCTP using invasive FFR, MRI, SPECT or even PET imaging as the reference standard (Tables 3,4). The advantage of CCTP imaging is an improvement in detecting the haemodynamic significance of CAD, adding incremental predictive value to CTCA-based coronary stenosis evaluation. The CORE320 trial, a prospective multicenter multinational diagnostic study including a total of 381 participants, demonstrated that combining stress CCTP imaging to anatomical evaluation of luminal stenosis substantially increased the overall diagnostic accuracy

and specificity to identify flow-limiting stenosis, defined as  $\geq 50\%$  stenosis by CA and causing perfusion defect by SPECT (37,39). This improvement has been demonstrated in patients with and without known CAD, at both patient and vessel levels (37,39).

Furthermore, the overall performance of CCTP imaging in the diagnosis of anatomic CAD (stenosis  $\geq 50\%$  at CA as determined with quantitative methods) was higher than that of SPECT, and was driven in part by a higher sensitivity for left main and multivessel disease (38).

More recently, a two-center prospective sub-study of the CORE320 trial demonstrated that the diagnostic performance of CCTP with whole-heart coverage and single-beat acquisition was comparable to that of dynamic myocardial MRI perfusion imaging (98).

Similar to the CORE320 trial, the regadenoson cross-over study, a randomized, multivendor, multicenter study including 110 patients comparing the accuracy of CCTP for the detection of myocardial ischemia against SPECT, demonstrated that regadenoson CCTP was non-inferior to SPECT for detecting reversible perfusion defect with an agreement rate of 0.87. By adding regadenoson CCTP imaging to CTCA evaluation, diagnostic accuracy improved from 69% to 85% with high sensitivity and specificity of 90% and 84%, respectively, which was mainly explained by a reduction in false positive rate (40).

Moreover, stress CCTP has been shown to improve the diagnostic performance of CTCA even in patients with high pre-test probability of CAD (99), heavily calcified coronary arteries or prior coronary revascularization (100,101).

Of note, according to a recent pooled analysis on a per-patient basis, dual-energy and dynamic quantitative CCTP tends to have a slightly higher sensitivity than static CCTP imaging (36). This may be related to a higher detection of subtle perfusion defects. Finally, semi-quantitative parameters such as the transmural perfusion ratio (TPR), determined as the ratio of the subendocardial to the mean subepicardial contrast attenuation, and myocardial reserve index (difference in attenuation between the stress and rest phases) have been proposed for static myocardial CCTP. They, however, have demonstrated lower diagnostic accuracy than standard visual qualitative analysis (75,79).

Recent meta-analyses have shown an additional value of functional CCTP over anatomic CTCA alone for the assessment of haemodynamically significant CAD. Takx *et al.* demonstrated that, at the patient level, stress CCTP was similar to stress MRI and PET, and better than SPECT and echocardiography for the detection of myocardial ischemia

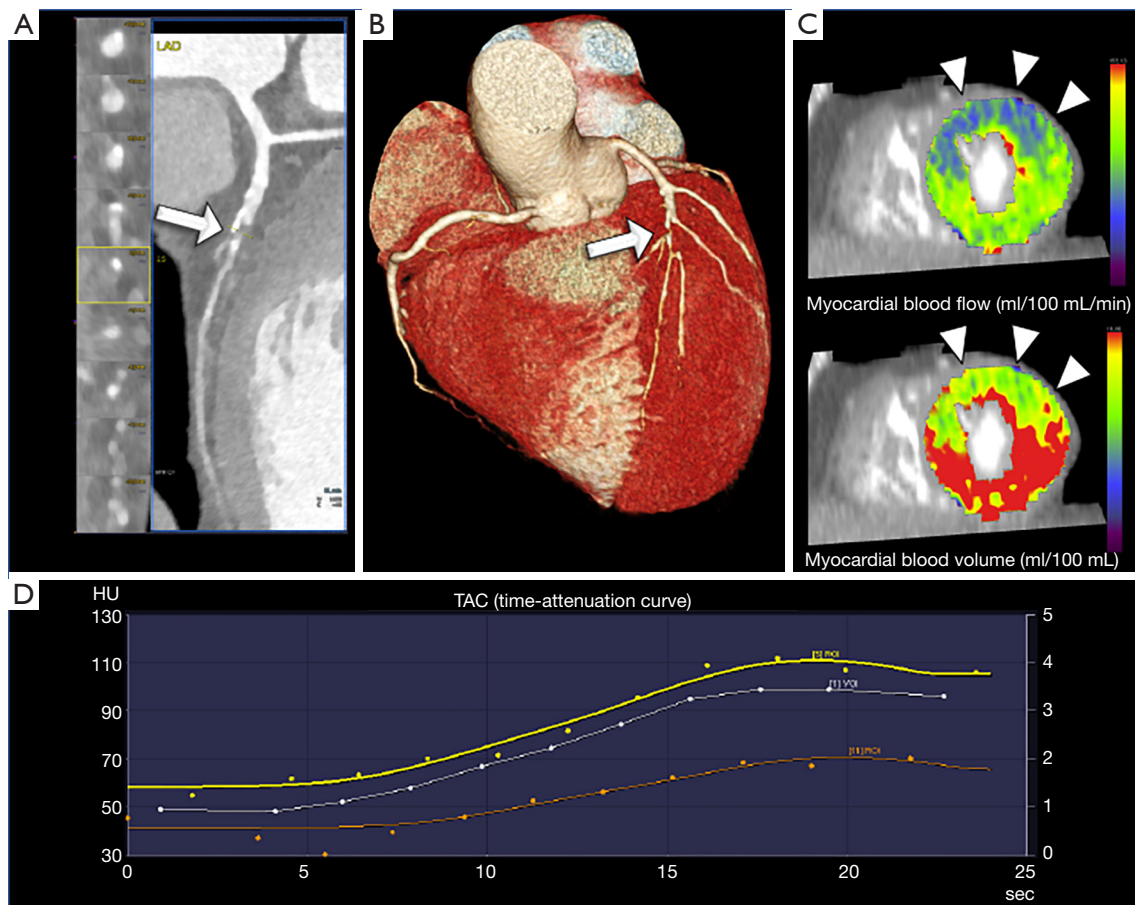


**Figure 4** Stress dynamic CT myocardial perfusion imaging. A 63-year-old diabetic male patient with multiple cardiovascular risk factors presented with atypical chest pain. Curved multiplanar (A) and 3D volume rendering technique (VRT, B) coronary CT angiography reconstructions show a mixed atherosclerotic plaque causing a critical stenosis (>70% luminal narrowing) at the middle segment of the left anterior descending artery (LAD) (arrows). (C) Three-dimensional color-coded short-axis CT perfusion map images at stress show perfusion defects in the territory of the LAD (antero-septal wall, anterior and antero-lateral wall) (arrowheads) with reduction of the myocardial blood flow (MBF, upper image) and myocardial blood volume (MBV, lower image). (D) The corresponding tissue time-attenuation curves (TACs) of the myocardium from several consecutive acquisitions throughout the cardiac cycle at the anterior wall (orange line), inferior wall (yellow line), and entire left ventricular myocardium (white line). Note the kinetics of the wash-in and wash-out of contrast media of the severely ischemic myocardium (orange line), with decreased wash-in and a reduced peak enhancement of the TAC. The corresponding value of the hemodynamic parameters derived from the TACs, demonstrates a significant reduction of MBF and MBV in the territory of the LAD, consistent with inducible ischemia. In the LAD territory, MBF was  $62.02 \pm 6.82$  mL/100 mL/min and MBV was  $10.21 \pm 0.95$  mL/100 mL; in the remote myocardium (inferior wall) MBF was  $105.86 \pm 8.57$  mL/100 mL/min and MBV was  $17.97 \pm 1.29$  mL/100 mL.

defined by FFR (102). In another larger meta-analysis including 5,330 patients, Celeng *et al.* demonstrated that both CCTP imaging and  $FFR_{CTA}$  yielded higher diagnostic performance than CTCA in detecting haemodynamically significant CAD, with FFR as a reference (103). High to excellent sensitivity for both CCTP and  $FFR_{CTA}$  and high specificity, especially for CCTP, have been demonstrated (103).

Dynamic CCTP has been initially validated in animal studies, showing a good correlation between quantitative dynamic-CT MBF values and invasive measurements of coronary blood flow, FFR, histopathology, and fluorescent microsphere (Table 4).

In recent clinical study, CT myocardial attenuation density was correlated with  $^{15}O$ -water PET MBF, the

**Table 2** Major differences of static and dynamic myocardial perfusion imaging

	Static CCTP	Dynamic CCTP
State-of-the art CT scanner technology	Required**	Required
Breath-hold time	Shorter (<10 s)	Longer (~20–30 seconds)
Radiation dose	Lower	Higher
Optimal acquisition time	Crucial	Less crucial
Evaluation of myocardial wall motion abnormalities	Yes*	No
Quantification of myocardial iodine concentration (mg/mL)	Yes**	No
Simultaneous coronary and myocardial perfusion evaluation	Yes	No
Analysis of myocardial perfusion	Qualitative/semi-quantitative**	Qualitative/semi-quantitative/quantitative (MBF and MBV)
Quantification of absolute CFR	No	Yes
Detection of diffuse ischemia in multivessel CAD	No	Yes
Evaluation of microvascular disease	No	Yes
Susceptibility to artefacts	Lower	Higher
Post-processing time	Shorter	Longer

\*, with retrospective ECG-gated acquisition; \*\*, with the dual- or multi-energy myocardial perfusion acquisition. CCTP, cardiac computed tomography perfusion; CAD, coronary artery disease; MBF, myocardial blood flow; MBV, myocardial blood volume; CFR, coronary flow reserve.

established clinical standard for MBF quantification (104). Several studies demonstrated improved diagnostic performance using indexed MBF normalized against remote myocardium, i.e., the ratio between the absolute MBF of ischemic coronary territories and segmental values of the remote myocardium (74,97,105–107).

Recently, a meta-analysis including a total of 482 patients demonstrated high diagnostic performance of dynamic CCTP to diagnose myocardial ischemia compared with clinically established reference standard (MRI, SPECT, PET perfusion and FFR). The pooled sensitivity and specificity of MBF were 83% and 90% at segment level and 93% and 83% (compared to 91% and 49% by CTCA) at patient level, respectively (108).

### **Prognostic value of cardiac CT perfusion**

Initial evidence pointing to improved prognostic value and better risk stratification for CCTP has been recently reported. Combining CTCA and CCTP was shown to confidently predict all-cause mortality, myocardial infarction, or coronary revascularization over a 2-year period (109). Moreover, stress dynamic CCTP provides

a predictive value that is incremental over clinical risk factors for major adverse cardiac events (MACE) and for the detection of coronary stenosis at CTCA (110–113). van Assen *et al.* (113) showed that quantification of index MBF (the ratio between territory and global MBF) was a better independent predictor of MACE, as compared to CTCA and  $FFR_{CTA}$ .

### **Radiation burden of cardiac CT perfusion**

Currently, it is possible to achieve a low-dose radiation exposure in clinical practice with the latest dose-reduction strategies of modern CT scanner, e.g., prospective ECG-triggered sequential scanning, wider anatomical coverage up to 320-slice, high pitch spiral acquisition, dose modulation, automated tube voltage selection, iterative image reconstruction software, and noise reduction filters. The effective radiation dose for a static single-phase CCTP scan generally is less than 5 mSv, which can be lower than the dose from CA (27,29,114) and approaches the average background radiation exposure in the United States of 3 mSv/y (27). Furthermore, an ultra-low dose protocol with an effective radiation dose as low as less than 1 mSv

**Table 3** Most relevant studies of static single- and dual-energy CCTP imaging

Author [year]	Patients No.	CT Technology	CCTP protocol	Stressor (dose)	Obstructive CAD prevalence, per patient (%)	Monovessel/ multivessel CAD (No.)	Average radiation dose (mSv)	Analysis basis	Reference standard	SE (%)	SP (%)	PPV (%)	NPV (%)
<b>Single-energy CCTP studies</b>													
Feuchtner et al. (29) [2011]	30	DS (2nd)	Stress/rest	Adenosine (0.14 mg/kg/min)	96 <sup>a</sup>	NA	0.93	Visual	MRI 1.5 T (for vessel)	96	88	93	94
Ko et al. (75) [2012]	40	320-slice	Rest/stress	Adenosine (0.14 mg/kg/min)	52.5 <sup>b</sup>	9/12	4.5	TPR	FFR (for vessel)	74	66	56	81
George et al. (76) [2012]	50	320-slice	Rest/stress/LE	Adenosine (0.14 mg/kg/min)	36 <sup>c</sup>	12/6	7.0	TPR	SPECT (for patient)	72	91	81	85
Bettencourt et al. (77) [2013]	101	64-slice	Stress/rest	Adenosine (0.14 mg/kg/min)	47.5 <sup>b</sup>	24/24	5.0*	Visual <sup>§</sup>	FFR (for patient)	89	83	80	90
Wong et al. (78) [2014]	75	320-slice	Rest/stress	Adenosine (0.14 mg/kg/min)	NA	NA	4.8	Visual + TAG <sup>§</sup>	FFR (for vessel)	97	84	76	98
Rochitte et al. [CORE320 study] (37) [2014]	381	320-slice	Rest/stress	Adenosine (0.14 mg/kg/min)	59 <sup>d</sup>	NA	5.31	Semiq	QCA + SPECT (for patient)	80	74	65	86
George et al. [CORE320 study] (38) [2014]	381	320-slice	Rest/stress	Adenosine (0.14 mg/kg/min)	60 <sup>d</sup>	76/153	NA	Semiq	QCA (for patient)	88	55	75	75
Yang et al. (79) [2015]	75	DS (2nd)	Stress/rest	Adenosine (0.14 mg/kg/min)	81 <sup>b</sup>	41/20	6.5	Visual	FFR (for patient)	89	86	96	63
Magalhães et al. [CORE320 study] (39) [2015]	381	320-slice	Rest/stress	Adenosine (0.14 mg/kg/min)	59 <sup>d</sup>	NA	NA	Visual <sup>§</sup>	FFR (for vessel)	80	95	92	87
Cury et al. [Regadenoson crossover study] (40) [2015]	110	Multivendor	Stress/rest	Regadenoson (0.4 mg)	NA	NA	17.7*	Semiq	QCA + SPECT (for patient)	78	73	64	85

**Table 3** (continued)

Table 3 (continued)

Author [year]	Patients No.	CT Technology	CCTP protocol	Stressor (dose)	Obstructive CAD prevalence, per patient (%)	Monovessel/ multivessel CAD (No.)	Average radiation dose (mSv)	Analysis basis	Reference standard	SE (%)	SP (%)	PPV (%)	NPV (%)
Dual-energy CCTP studies													
Ko et al. (31) [2012]	45	DS (1st)	Rest/stress	Adenosine (0.14 mg/kg/min)	93 <sup>d</sup>	20/22	5.7	Iodine map (for vessel)	QCA	89	74	80	85
Meinel et al. (80) [2014]	55	DS (2nd)	Stress/rest/LE	Adenosine (0.14 mg/kg/min); regadenoson (0.4 mg)	NA	NA	7.1	Iodine map (for segment)	SPECT	99	97	92	100
Deigado et al. (81) [2013]	56	DS (2nd)	Stress/rest/LE	Adenosine (0.14 mg/kg/min)	27 <sup>e</sup>	11/4	5.2	Iodine map (for segment)	MRI 1.5T	76	99	89	98
Kim et al. (82) [2014]	50	DS (2nd)	Stress/rest <sup>e</sup>	Adenosine (0.14 mg/kg/min)	50 <sup>e</sup>	NA	6.5	Iodine map (for segment)	MRI 1.5T	77	94	53	98
Ko et al. (83) [2014]	40	DS (1st)	CTCA/stress/rest	Adenosine (0.14 mg/kg/min)	NA	NA	4.6	Iodine map (for vessel) <sup>§</sup>	QCA + MRI 3T	87	79	71	91
Ko et al. (84) [2014]	100	DS (1st)	Rest/stress	Adenosine (0.14 mg/kg/min)	82 <sup>d</sup>	36/46	4.2	Iodine map (for vessel) <sup>§</sup>	QCA + MRI 1.5T and 3T	88	79	73	91

<sup>a</sup>, the rest phase was acquired in the single-energy mode; <sup>\*</sup>, global radiation dose of the stress-rest protocol; <sup>§</sup>, accuracy of CT perfusion integrated with the coronary anatomic data; <sup>¶</sup>, data regarding coronary stenosis >70% by QCA performed in 25 out of 30 patients; <sup>b</sup>, data regarding FFR-hemodynamically significant stenosis; <sup>°</sup>, data regarding coronary stenosis ≥50% by CTCA; <sup>°</sup>, data regarding coronary stenosis ≥50% by QCA; <sup>°</sup>, data regarding coronary stenosis >50% by CTCA. CCTP, cardiac computed tomography perfusion; 1st and 2nd, first and second generation; CAD, coronary artery disease; CTCA, computed tomography coronary angiography acquired in the single-energy mode; DS, Dual-Source scanner; FFR, fractional flow reserve; LE, late-enhancement; MRI, magnetic resonance imaging; NA, non-assessable; No, patients' number; NPV, negative predictive value; PPV, positive predictive value; QCA, quantitative coronary angiography; SE, sensitivity; SP, specificity; Semicq, semiquantitative analysis using a stress score; SPECT, myocardial perfusion scan; TPR, Transmural perfusion ratio; TAG, transmural attenuation gradient.

Table 4 Most relevant studies of dynamic CCTP imaging studies on animal and humans

Author [year]	No.	CT technology	CCTP protocol	Stressor (dose)	Average radiation dose (mSv)	Analysis basis	Reference standard	SE (%)	SP (%)	PPV (%)	NPV (%)
Studies on animals											
Bamberg et al. (85) [2012]	7 pigs	DS (2nd)	Rest/stress	Adenosine (0.14 mg/kg/min)	10.6	Quantitative MBF	Microsphere MBF	-	-	-	-
Rossi et al. (86) [2013]	7 pigs	DS (2nd)	Stress	Adenosine (0.50 mg/kg/min)	17.1	Quantitative MBF	CBF and FFR	-	-	-	-
Schwarz et al. (87) [2013]	6 pigs	DS (2nd)	Rest/stress*	Adenosine (0.14 mg/kg/min)	11.3 (dynamic) + 0.88 (static)	Quantitative MBF + attenuation values (HU)	Microsphere MBF	-	-	-	-
Bamberg et al. (88) [2014]	12 pigs	DS (2nd)	Rest/stress	Adenosine (0.14 mg/kg/min)	NA	Quantitative MBF, MBV, $K_{trans}$	Histopathology, microsphere MBF	-	-	-	-
Pelgrim et al. (89) [2017]	5 pigs	DS (2nd)	Stress	-	NA	Quantitative MBF	FFR and Microsphere MBF	-	-	-	-
Studies on humans											
Ho et al. (90) [2010]	35	DS (2nd)	Stress/CTCA	Dipyridamole (0.56 mg/kg in 4 min)	9.1	Quantitative MBF	SPECT (for segments)	83	78	79	82
Bamberg et al. (30) [2011]	33	DS (2nd)	CTCA/stress	Adenosine (0.14 mg/kg/min)	10	Quantitative MBF	FFR <sup>§</sup> (for vessel)	93	87	75	97
Wang et al. (91) [2012]	30	DS (2nd)	CTCA/stress	Adenosine (0.14 mg/kg/min)	9.5	Visual Quantitative MBF and MBV	QCA + SPECT (for vessel)	100	76	54	100
Greif et al. (92) [2013]	65	DS (2nd)	CTCA/stress	Adenosine (0.14 mg/kg/min)	9.7	Quantitative MBF	FFR (for vessel)	95	74	49	98
Huber et al. (93) [2013]	32	256-slice	Stress	Adenosine (0.14 mg/kg/min)	9.5	Quantitative MBF	FFR (for vessel)	76	100	100	91
Bamberg et al. (94) [2014]	31	DS (2nd)	CTCA/stress	Adenosine (0.14 mg/kg/min)	11.08	Quantitative MBF and MBV	MRI 3T (for vessel)	100	75	92	100
Rossi et al. (95) [2014]	80	DS (2nd)	CTCA/stress	Adenosine (0.14 mg/kg/min)	9.4	Quantitative MBF	FFR (for vessel)	88	90	77	95
Coenen et al. (96) [2017]	74	DS (2nd and 3rd)	CTCA/stress	Adenosine (0.14 mg/kg/min)	9.3	Absolute MBF, Index MBF	FFR (for vessel)	75	61	63	73
Rossi et al. (74) [2017]	115	DS (2nd)	CTCA/stress, CTCA	Adenosine (0.14 mg/kg/min)	6 (at 80 kV)-10.3 (at 100 kV)	Quantitative relative endocardial MBF <sup>°</sup>	QCA or FFR (for vessel)	88	84	64	95
Yi et al. (97) [2019]	60	DS (3rd)	Stress/CTCA	Adenosine (0.16 mg/kg/min)	NA	Quantitative absolute endocardial MBF <sup>°</sup>	75	88	68	91	
						MBF/highest segmental endocardial MBF <sup>°</sup>	QCA or FFR (for vessel)	74	94	88	85

\*, the rest/stress protocol was acquired in both dynamic and high pitch static acquisitions; <sup>§</sup>, accuracy of CT perfusion integrated with the coronary anatomic data; <sup>°</sup>, perfusion parameters obtained by semiautomatic analysis. CCTP, cardiac computed tomography perfusion; 2nd, second generation; 3rd, third generation; CBF, coronary blood flow; CTCA, computed tomography coronary angiography acquired in the static mode; DS, dual-source scanner; FFR, fractional flow reserve; MRI, magnetic resonance imaging; MBF, myocardial blood flow; MBV, myocardial blood volume; NA, non-assessable; No, number; NPV, negative predictive value; PPV, positive predictive value; QCA, quantitative coronary angiography; SE, sensitivity; SP, specificity; SPECT, myocardial perfusion scan.

has been recently reported using prospectively ECG-triggered turbo high pitch spiral acquisition, which allows the acquisition of the entire heart within a single heartbeat in approximately one quarter of second (115).

A major concern is the higher radiation burden inherent to the dynamic CCTP protocols, which require a time-resolved acquisition of multiple phases. According to a recent meta-analysis, dynamic CCTP is associated with a median ionizing radiation of 9.45 mSv (range, 5.3–10.5 mSv) for a single scan, which is nonetheless comparable with that of traditional nuclear imaging techniques (108).

To overcome such limitations, the use of a low tube voltage protocol (80-kV/370-mA) instead of a conventional protocol (100-kV/300-mAs) enables 40% dose reduction without affecting image quality and MBF quantification (116). Moreover, other methods such as half-scan acquisition, new first-pass analysis using only two first-pass scans, tube current modulation, and statistical iterative reconstruction technique could substantially reduce effective radiation dose (23).

## CTCA-derived FFR ( $FFR_{CTA}$ )

### Overview of $FFR_{CTA}$ technology

Due to the non-invasive nature of CTCA, the application of CFD algorithms on CTCA-derived 3D arterial models has received wide clinical interest. According to this approach, haemodynamic factors such as flow and pressure are not known a priori, thus parameter models regarding the cardiac output, the resistance of the coronary microcirculation and the pressure of the systemic circulation are coupled with the flow domain of the aortic root and the epicardial arteries, where the governing equations of flow dynamics are solved and can consequently provide  $FFR_{CTA}$  calculations.

There are four approaches to non-invasive, in-silico CTCA-derived FFR estimation: (I) full-order modeling of haemodynamics; (II) reduced-order/steady-state modeling; (III) hybrid models; and (IV) deep machine learning algorithms, including both commercially available solutions and technologies still in development phase (117,118). All these techniques are based on a patient-specific anatomic coronary artery 3D model, obtained via a preliminary semiautomated process of segmentation and contouring. The full-order approaches require a complete model of the entire coronary tree, and an additional physiology model of the coronary microcirculation fluid dynamics (derived from patient-specific boundary conditions),

from which a coronary blood flow model is derived. This process is computationally demanding, requiring off-site supercomputers in core laboratories. For this reason, simpler models have been introduced, that are either segment-specific and/or rely on a generalized (non-patient-specific) haemodynamic models. This allows near real time FFR estimation using workstations at the point of care, but lacks accuracy in small segments, near side branches and in eccentric lesions (119).

To date, the only commercially available FFR computation from CTCA solution known as  $FFR_{CT}$  is available as a web-based service marketed by HeartFlow, Inc. (Redwood City, California, USA). According to the National Institute for Health and Care Excellence (NICE) guidance on the subject (120), HeartFlow provides an end-to-end service that includes anonymization at the source and human intervention (*Figures 5,6*).

Some standalone computational methodology has been proposed for non-invasive calculation of FFR (119,121-124). SmartFFR is based on a transient blood flow simulation and the calculation of the pressure-flow curve between the distal and proximal region of the coronary artery. The novelty of SmartFFR lies in the fact that it can be effectively applied on arterial bifurcations and it can be calculated in just a few minutes, without the need of clinical tests besides a good quality CTCA. There is both a cloud-based platform and a standalone version (119,121,122) (*Figures 6,7*).

The specific value of systems that can be added to a normal server or laptop concerns direct management by a single operator during the evaluation process of the CT images. Another important advantage is rapid analysis, necessitating no more than a few minutes (121).

The main limitation for all existing 3D methodologies is that, if an error is generated, this can be propagated along the entire workflow of the reconstruction process, significantly altering the calculated blood flow simulation results (125).

### Diagnostic accuracy of $FFR_{CTA}$

Three major multi-center studies (DISCOVER-FLOW, DeFACTO and HeartFlow NXT) have provided clinical validation of  $FFR_{CTA}$ , directly comparing their computational results to the measured invasive FFR values, and producing promising results that can be applied in clinical settings (126-128).

The DISCOVER-FLOW study exhibited a good correlation between  $FFR_{CTA}$  and standard FFR ( $r=0.68$ )

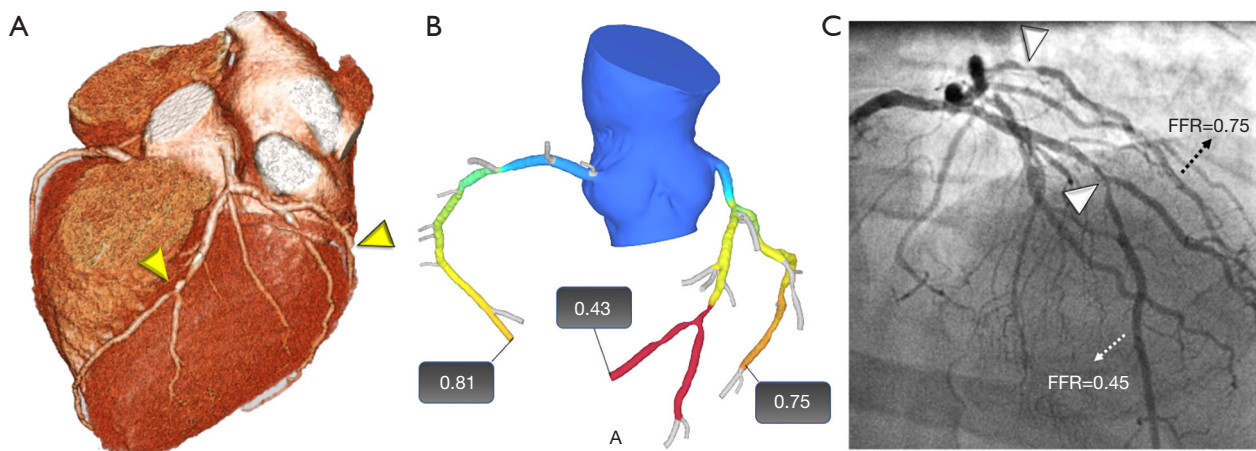


**Figure 5** Case example of HeartFlow— $FFR_{CT}$ . (A) 3D volume rendering technique (VRT) coronary CT angiography reconstruction shows critical stenoses (>70% luminal narrowing) of the left anterior descending artery (LAD) at the diagonal bifurcation and of the 2nd obtuse marginal branch (OM), arrowheads. (B) Computation of  $FFR_{CT}$  demonstrates that LAD and OM stenoses are hemodynamically significant with  $FFR_{CT}$  value of 0.43 and 0.75, respectively. (C) Invasive coronary angiography confirms the critical LAD and OM stenoses (arrowheads). Note the close correspondence between  $FFR_{CT}$  and invasively-measured FFR values.

with respective diagnostic accuracy, sensitivity, specificity, positive predictive value and negative predictive value for predicting hemodynamically significant stenoses ( $FFR \leq 0.8$ ) being 84%, 88%, 82%, 74% and 92%, respectively (126).

Furthermore, when compared to cases of  $\geq 50\%$  stenosis detected solely by CTCA,  $FFR_{CTA}$  showed superior discrimination (AUC: 0.90 *vs.* 0.75,  $P=0.001$ ). In the DeFACTO study, stable CAD patients underwent CTCA,  $FFR_{CTA}$  and CA with FFR measurement (127). The per patient diagnostic accuracy, sensitivity, specificity, positive predictive value and negative predictive value for predicting an  $FFR \leq 0.8$  were 73%, 90%, 54%, 67%, and 84%, respectively. Good correlation was also found between the two methods ( $r=0.68$ ). The most recent HeartFlow NXT, further validated  $FFR_{CTA}$ , using updated proprietary software which included refined mathematical models, further increasing automation, image quality assessment, and image segmentation (128). Diagnostic accuracy, sensitivity, specificity, positive predictive value and negative predictive value for predicting an  $FFR \leq 0.8$  were 81%, 86%, 79%, 65%, and 93%, respectively on a per-patient basis and 86%, 84%, 86%, 61%, and 95%, respectively, on a per-vessel basis. Finally, a good correlation was found between  $FFR_{CTA}$  and FFR ( $r=0.82$ ) (128). The PLATFORM study focused on the clinical outcomes of FFR by CTCA-guided diagnostic strategies compared to the standard care in CAD-suspected patients, providing insight on the clinical

utilization of  $FFR_{CTA}$  (129). Following the findings of the PLATFORM trial, the PROMISE study concluded that if CA is performed only in patients with  $FFR_{CTA} \leq 0.8$ , the rate of finding unobstructed coronaries at CA could decrease by 44% and, at the same time, the rate of CA leading to appropriate revascularization would increase by 24% (130).

Sensitivity and specificity of these techniques, however, have been shown to vary in different cohorts, due to differences in sample sizes and study population characteristics (Table 5).

In a recent meta-analysis including 908 vessels in 5 studies,  $FFR_{CTA}$  showed an overall per-vessel diagnostic accuracy of 82% against invasive FFR (134). However, high variability of the diagnostic accuracy of  $FFR_{CTA}$  has been observed across the entire spectrum of the disease. Regarding vessels with  $FFR_{CTA} > 0.90$ , the vast majority (97.9%) met the guideline FFR criterion for deferral ( $FFR > 0.80$ ), whereas for vessels with  $FFR_{CTA} < 0.60$ , 86.4% met the FFR criterion ( $FFR \leq 0.8$ ) for PCI. Regarding the  $FFR_{CTA}$  values laying in between the thresholds, there was less certainty on whether invasive FFR would actually meet the criteria for stenosis deferral or revascularization (134).

Finally,  $FFR_{CTA}$  exhibits an acceptable accuracy for the detection of haemodynamically relevant lesions without an additional radiation exposure (127), and being associated with equivalent clinical outcomes, similar quality-of-life and lower costs, when compared with usual care over 1-year

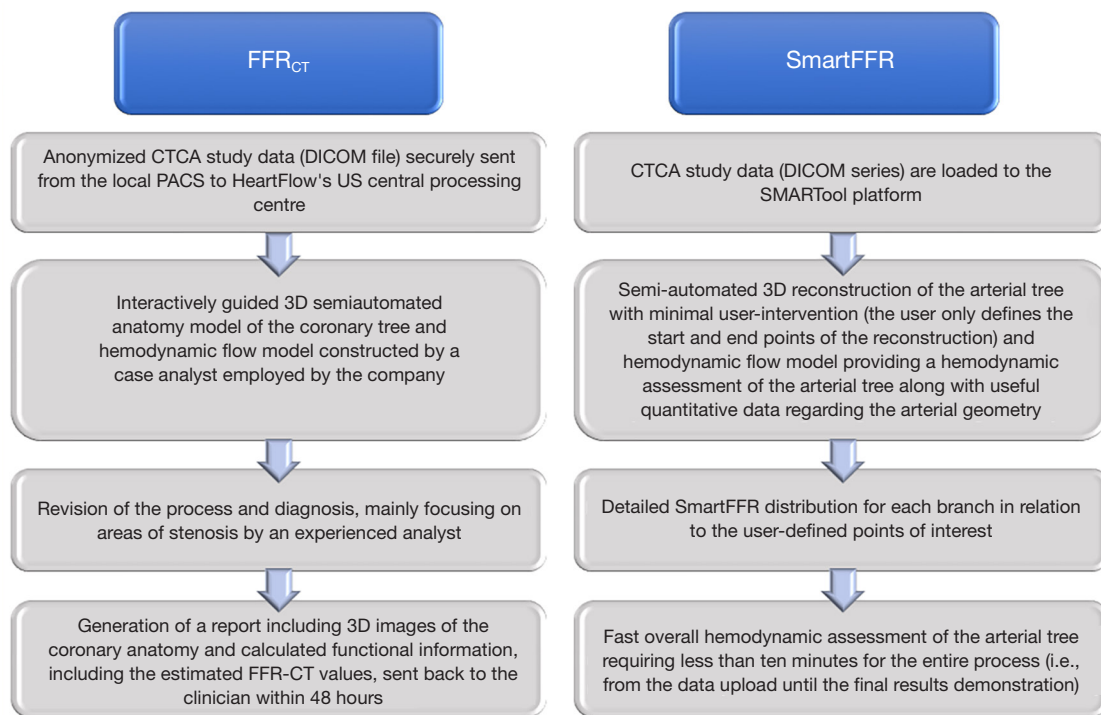


**Figure 6** Workflow differences between the HeartFlow— $FFR_{CT}$  and the SMARTool—SmartFFR analyses.

follow-up (129).

### Real-world role of cardiac CT perfusion and $FFR_{CTA}$ : limits and perspectives

Compared to other non-invasive functional imaging techniques, both static and dynamic CCTP offer the unique advantage to assess myocardial perfusion defects together with coronary anatomy in the same examination. Perfusion defects are matched with patient-specific coronary artery tree reconstruction, taking into account individual vessel anatomy, coronary artery distribution, presence, extent and type of coronary atherosclerotic plaques, and with specific identification of coronary stenoses. Therefore, the main strength of CT-based functional methods is a fully integrated anatomical/functional analysis at individual level. The knowledge of atherosclerotic plaque characteristics and plaque burden when assessing myocardial perfusion adds clinical value. In fact, it has been demonstrated that specific plaque features (e.g., positive remodeling, low attenuation, spotty calcification, as well as low-density noncalcified plaque volume), which are also associated with the risk of future coronary syndromes, reflect an intrinsic propensity to

ischemia independent of stenosis severity when compared to FFR (15,135-137). Although not fully elucidated, the main mechanisms underlying the interactions between multiple plaque characteristics and lesion-specific ischemia include endothelial dysfunction, vascular inflammation, and altered shear stress patterns, which cause a shift in the balance of endothelial vasodilators and vasoconstrictors, thereby promoting ischemia during physiological stress (138).

Iodinated contrast materials used for CT express a pharmacodynamics similar to gadolinium-based extracellular media used for MRI. However, dynamic CCTP is not affected by the non-linear relationship between the measured myocardial signal intensity and myocardial contrast concentration, which may challenge accurate quantification of MBF in gadolinium MRI perfusion imaging (23). Other advantages of stress CCTP compared to MRI is the possibility to safely scan patients with active implanted medical devices, its wider availability, lower cost and quicker acquisition time. Furthermore, CCTP allows for a physiological noncorrupted 12-lead ECG monitoring during stress imaging, which is challenging in MRI.

CCTP offers several advantages in respect to nuclear imaging SPECT due to its higher temporal (up to 66 ms)

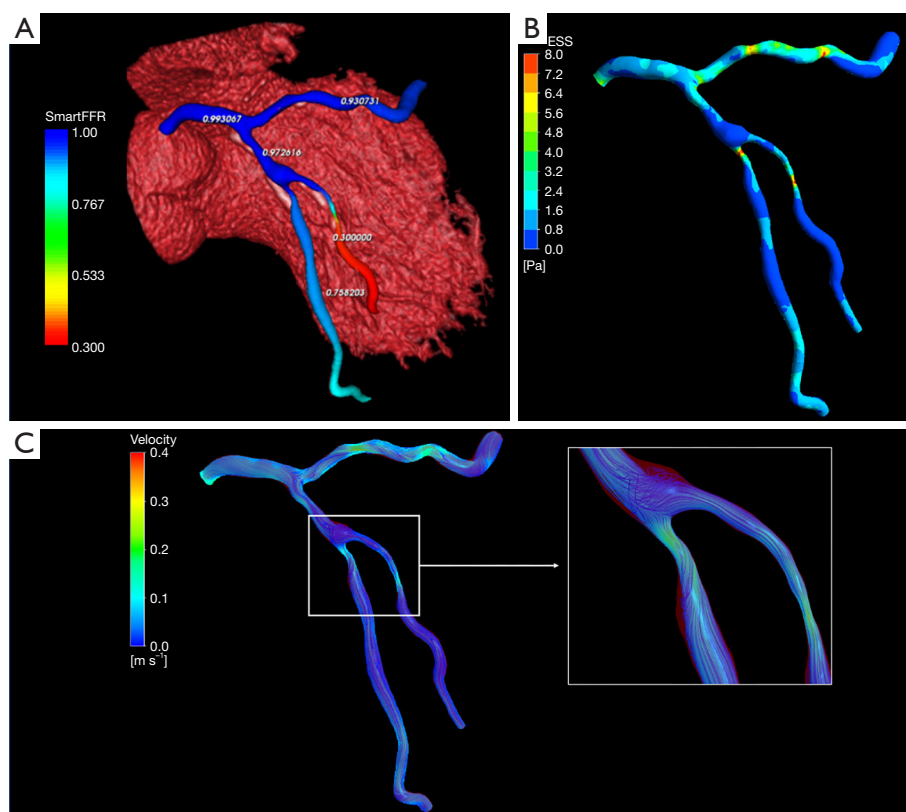


**Figure 7** Case example of SMARTool—SmartFFR. (A) Representative non-invasive CT volume rendering with 3D reconstruction of the left coronary artery and calculated SmartFFR values. Calculation is achieved in few minutes fully automatically. (B) Distribution of shear stress on the endothelial membrane of the reconstructed coronary arteries. Regions of increased stenosis present high endothelial shear stress (ESS) values expressed in Pascal (Pa), while regions of low ESS are more prone for disease development and progression. (C) Blood flow velocity (ms<sup>-1</sup>) streamlines after blood flow modelling. At the regions of bifurcation or stenoses (magnification box), recirculation zones are observed which are responsible for disease progression.

**Table 5** Actual diagnostic performance of computational FFR<sub>CTA</sub> when compared with invasive FFR in detecting physiologically significant lesions that need revascularization (cut-off  $\leq 0.80$ )

Studies	Sample size [patients, vessels]	Pearson correlation coefficient	Agreement (Bias $\pm$ SD: virtual index vs. FFR)	Overall diagnostic accuracy	AUC
DISCOVER-FLOW* [2011] (126)	103 [159]	0.68	0.02 $\pm$ 0.116	84% (per vessel)	0.90
DeFACTO* [2012] (127)	252 [407]	0.63	0.06	73% (per vessel)	0.81
HeartFlow NXT* [2014] (128)	251 [484]	0.82	0.02 $\pm$ 0.074	86% (per vessel)	0.93
Kim <i>et al.</i> [2014] (131)	44	0.60	0.006	77%	–
Renker <i>et al.</i> [2014] (132)	53	0.66	–	–	0.92
Coenen <i>et al.</i> [2015] (133)	106 [189]	0.59	–0.04 $\pm$ 0.13	74.6%	0.83
Kruk <i>et al.</i> [2016] (123)	90 [96]	0.67	–0.01 $\pm$ 0.095	74% (per vessel)	0.83
Ko <i>et al.</i> [2017] (124)	42 [78]	0.57	–0.065 $\pm$ 0.137	83.9% (per vessel)	0.88

\*, multicenter studies. FFR, fractional flow reserve; FFR<sub>CTA</sub>, fractional flow reserve from computed tomography angiography; AUC, area under the ROC curve; SD, standard deviation.

and spatial resolution ( $\leq 0.3$  mm), allowing detection of even small subendocardial area of ischemic or necrotic myocardium (23).

Despite these potential advantages, a significant drawback for both static and dynamic CCTP imaging is a low contrast-to-noise ratio (CNR) and the possibility of imaging artifacts linked to beam-hardening, partial volume effects, cardiac motion, and breathing. However, several dedicated reconstruction and motion correction algorithms are available (23,34).

Quantitative dynamic CCTP may offer some important advantages compared to static CCTP and SPECT in assessing balanced ischemia in the context of diffuse coronary atherosclerosis or multivessel obstructive CAD with global left ventricular impairment of MBF and CFR. Another clinical scenario worthy of quantitative CCTP is the evaluation of myocardial ischemia in patients with microvascular dysfunction and absence of obstructive CAD, where reduced hyperaemic MBF can be demonstrated, similar to PET imaging. Moreover, quantitative evaluation of MBF and MBV by dynamic CCTP may evaluate the functional importance of collateral circulation in coronary chronic total occlusions.

It should be noted, however, that differences in the optimal cut-off value of impaired MBF for detecting myocardial ischemia by dynamic CCTP have been reported, related to study design, scanner technology, acquisition protocol, post-processing elaboration, standard of reference applied, and, last but not least, individual coronary risk profile (23,33,36). Moreover, underestimation of absolute MBF and CFR values derived from dynamic CCTP imaging has been demonstrated, although in the documented range by PET studies (23,33,72). Sub-optimal temporal sampling frequencies of dynamic CCTP of the intracapillary first pass of contrast during hyperaemia and low extraction of iodine into the normal myocardium may partly explain these differences. Individual difference in vasodilator response and the known vasodilatory effect of iodinated contrast agents may be other possible explanations (72,74).

Of note, the more significant advantage of  $FFR_{CTA}$  over static and dynamic CCTP imaging is that only one scan at rest is required for evaluation of both coronary anatomy and lesion-specific ischemia, with no additional contrast or medications, whereas a stepwise approach with combination of the rest and stress phases is obligatory for the CCTP imaging.

Major limitations of  $FFR_{CTA}$  are the off-site and rather

time-consuming core-laboratory analysis using a super-computer and the high computational costs of about £700 for a single test (120). Moreover, the large variation in study outcomes is also another point of concern. Finally, heavy calcifications, arrhythmia and tachycardia may affect both CTCA and  $FFR_{CTA}$  image quality. In one study based on 116 patients with acute chest pain, 48 (41.4%) CTCA datasets were not included for  $FFR_{CTA}$  analysis due to motion artifacts, severe calcium blooming artifacts or excessive image noise (139). In another clinical study conducted in real clinical setting,  $FFR_{CTA}$  was measured in 43 out of 48 patients (89.6%) and the technical reasons were the image artifacts, transmission error and severe calcifications (140). The same reasons of unsuccessful  $FFR_{CTA}$  calculation was found in another study (92% inclusion of patients—187 out of 204) (141). Thus, the main conclusion about  $FFR_{CTA}$  feasibility is that it is strongly affected by image artifacts such as coronary motion or misalignment artifacts, transmission and registration errors, and finally blooming artifacts caused by severe calcifications. These factors may limit the applicability of non-invasive calculation of  $FFR$  in low-to-intermediate risk population than in high-risk patients with severe calcifications.

## Conclusions

Both qualitative and quantitative CCTP imaging and  $FFR_{CTA}$  have widened the clinical usefulness of CCT by improving its specificity and positive predictive value for evaluating the functional significance of coronary stenoses, with a concomitant reduction in false positives and unnecessary angiograms. Considerable variation in techniques and reference standards for CCTP to diagnose myocardial ischemia has emerged. Larger studies are necessary to standardize imaging protocols and interpretation, and to validate adequate databases of normal values of dynamic perfusion data, including separate metrics for men and women, similarly to nuclear imaging.

Finally,  $FFR_{CTA}$  has gathered a very large validation dataset and could potentially alter clinical practice by providing a non-invasive approach to the functional assessment of coronary stenoses.  $FFR_{CTA}$  might be used to screen patients with suspected obstructive CAD and to provide time and contrast-sparing information to the interventional cardiologist, allowing focused and simplified PCI in appropriate patients.

CCTP and  $FFR_{CTA}$  will continue to receive attention from the cardiovascular research community in the near

future, evolving from experimental imaging modalities to a core technology for clinical decision making of patients with suspected or known CAD.

## Acknowledgments

*Funding:* None.

## Footnote

*Provenance and Peer Review:* This article was commissioned by the Guest Editor (Filippo Cademartiri) for the series “Clinical Impact of Cardiac CT in Clinical Practice” published in *Cardiovascular Diagnosis and Therapy*. The article was sent for external peer review organized by the Guest Editor and the editorial office.

*Conflicts of Interest:* All authors have completed the ICMJE uniform disclosure form (available at <http://dx.doi.org/10.21037/cdt-20-414>). The series “Clinical Impact of Cardiac CT in Clinical Practice” was commissioned by the editorial office without any funding or sponsorship. AIS reports grants from FORTH during the conduct of the study. FC serves as an unpaid editorial board member of *Cardiovascular Diagnosis and Therapy* from Jul 2019 to Jun 2021. FC served as the unpaid Guest Editors of the series. The other authors have no other conflicts of interest to declare.

*Ethical Statement:* The authors are accountable for all aspects of the work in ensuring that questions related to the accuracy or integrity of any part of the work are appropriately investigated and resolved.

*Open Access Statement:* This is an Open Access article distributed in accordance with the Creative Commons Attribution-NonCommercial-NoDerivs 4.0 International License (CC BY-NC-ND 4.0), which permits the non-commercial replication and distribution of the article with the strict proviso that no changes or edits are made and the original work is properly cited (including links to both the formal publication through the relevant DOI and the license). See: <https://creativecommons.org/licenses/by-nc-nd/4.0/>.

## References

- Mantini C, Maffei E, Toia P, et al. Influence of image reconstruction parameters on cardiovascular risk reclassification by Computed Tomography Coronary Artery Calcium Score. *Eur J Radiol* 2018;101:1-7.
- Neglia D, Rovai D, Caselli C, et al. Detection of significant coronary artery disease by noninvasive anatomical and functional imaging. *Circ Cardiovasc Imaging* 2015;8:e002179.
- Cademartiri F, Romano M, Seitun S, et al. Prevalence and characteristics of coronary artery disease in a population with suspected ischemic heart disease using CT coronary angiography: correlations with cardiovascular risk factors and clinical presentation. *Radiol Med* 2008;113:363-72.
- Maffei E, Seitun S, Martini C, et al. CT coronary angiography and exercise ECG in a population with chest pain and low-to-intermediate pre-test likelihood of coronary artery disease. *Heart* 2010;96:1973-9.
- Cademartiri F, La Grutta L, Palumbo A, et al. Computed tomography coronary angiography vs. stress ECG in patients with stable angina. *Radiol Med* 2009;114:513-23.
- Maffei E, Seitun S, Guaricci AI et al. Chest pain: coronary CT in the ER. *Br J Radiol* 2016;89:20150954.
- Blanke P, Weir-McCall JR, Achenbach S, et al. Computed Tomography Imaging in the Context of Transcatheter Aortic Valve Implantation (TAVI)/Transcatheter Aortic Valve Replacement (TAVR): An Expert Consensus Document of the Society of Cardiovascular Computed Tomography. *JACC Cardiovasc Imaging* 2019;12:1-24.
- Maffei E, Palumbo A, Martini C, et al. Diagnostic accuracy of 64-slice computed tomography coronary angiography in a large population of patients without revascularisation: registry data and review of multicentre trials. *Radiol Med* 2010;115:368-84.
- Yang L, Zhou T, Zhang R, et al. Meta-analysis: diagnostic accuracy of coronary CT angiography with prospective ECG gating based on step-and-shoot, Flash and volume modes for detection of coronary artery disease. *Eur Radiol* 2014;24:2345-52.
- Maffei E, Seitun S, Palumbo A, et al. Prognostic value of Morise clinical score, calcium score and computed tomography coronary angiography in patients with suspected or known coronary artery disease. *Radiol Med* 2011;116:1188-202.
- Cademartiri F, Seitun S, Romano M, et al. Prognostic value of 64-slice coronary angiography in diabetes mellitus patients with known or suspected coronary artery disease compared with a nondiabetic population. *Radiol Med* 2008;113:627-43.
- Maffei E, Seitun S, Martini C, et al. Prognostic value of computed tomography coronary angiography in patients

- with chest pain of suspected cardiac origin. *Radiol Med* 2011;116:690-705.
13. Aldrovandi A, Maffei E, Palumbo A, et al. Prognostic value of computed tomography coronary angiography in patients with suspected coronary artery disease: a 24-month follow-up study. *Eur Radiol* 2009;19:1653-60.
  14. Andreini D, Pontone G, Mushtaq S, et al. A long-term prognostic value of coronary CT angiography in suspected coronary artery disease. *JACC Cardiovasc Imaging* 2012;5:690-701.
  15. Motoyama S, Ito H, Sarai M, et al. Plaque Characterization by Coronary Computed Tomography Angiography and the Likelihood of Acute Coronary Events in Mid-Term Follow-Up. *J Am Coll Cardiol* 2015;66:337-46.
  16. SCOT-HEART Investigators. CT coronary angiography in patients with suspected angina due to coronary heart disease (SCOT-HEART): an open-label, parallel-group, multicentre trial. *Lancet* 2015;385:2383-91. Erratum in: *Lancet* 2015;385:2354.
  17. Douglas PS, Hoffmann U, Patel MR, et al. Outcomes of anatomical versus functional testing for coronary artery disease. *N Engl J Med* 2015;372:1291-300.
  18. Newby DE, Adamson PD, Berry C, et al. Coronary CT Angiography and 5-Year Risk of Myocardial Infarction. *N Engl J Med* 2018;379:924-33.
  19. Knuuti J, Wijns W, Saraste A, et al. 2019 ESC Guidelines for the diagnosis and management of chronic coronary syndromes. *Eur Heart J* 2020;41:407-77.
  20. Kim HL, Kim YJ, Lee SP, et al. Incremental prognostic value of sequential imaging of single-photon emission computed tomography and coronary computed tomography angiography in patients with suspected coronary artery disease. *Eur Heart J Cardiovasc Imaging* 2014;15:878-85.
  21. Gimelli A, Liga R, Duce V, et al. Accuracy of myocardial perfusion imaging in detecting multivessel coronary artery disease: A cardiac CZT study. *J Nucl Cardiol* 2017;24:687-95.
  22. Gimelli A, Liga R, Clemente A, et al. Appropriate choice of stress modality in patients undergoing myocardial perfusion scintigraphy with a cardiac camera equipped with solid-state detectors: the role of diabetes mellitus. *Eur Heart J Cardiovasc Imaging* 2018;19:1268-75.
  23. Seitun S, De Lorenzi C, Cademartiri F, et al. CT Myocardial Perfusion Imaging: A New Frontier in Cardiac Imaging. *Biomed Res Int* 2018;2018:7295460.
  24. Neumann FJ, Sousa-Uva M, Ahlsson A, et al. 2018 ESC/EACTS Guidelines on myocardial revascularization. *Eur Heart J* 2019;40:87-165.
  25. Maffei E, Martini C, Rossi A, et al. Diagnostic accuracy of second-generation dual-source computed tomography coronary angiography with iterative reconstructions: a real-world experience. *Radiol Med* 2012;117:725-38.
  26. Maffei E, Martini C, Tedeschi C, et al. Diagnostic accuracy of 64-slice computed tomography coronary angiography in a large population of patients without revascularisation: registry data on the comparison between male and female population. *Radiol Med* 2012;117:6-18.
  27. Maffei E, Martini C, De Crescenzo S, et al. Low dose CT of the heart: a quantum leap into a new era of cardiovascular imaging. *Radiol Med* 2010;115:1179-207.
  28. Kurata A, Mochizuki T, Koyama Y, et al. Myocardial perfusion imaging using adenosine triphosphate stress multi-slice spiral computed tomography: alternative to stress myocardial perfusion scintigraphy. *Circ J* 2005;69:550-7.
  29. Feuchtner G, Goetti R, Plass A, et al. Adenosine stress high-pitch 128-slice dual-source myocardial computed tomography perfusion for imaging of reversible myocardial ischemia: comparison with magnetic resonance imaging. *Circ Cardiovasc Imaging* 2011;4:540-9.
  30. Bamberg F, Becker A, Schwarz F, et al. Detection of hemodynamically significant coronary artery stenosis: incremental diagnostic value of dynamic CT-based myocardial perfusion imaging. *Radiology* 2011;260:689-98.
  31. Ko SM, Choi JW, Hwang HK, et al. Diagnostic performance of combined noninvasive anatomic and functional assessment with dual-source CT and adenosine-induced stress dual-energy CT for detection of significant coronary stenosis. *AJR Am J Roentgenol* 2012;198:512-20.
  32. Seitun S, Castiglione Morelli M, Budaj I, et al. Stress Computed Tomography Myocardial Perfusion Imaging: A New Topic in Cardiology. *Rev Esp Cardiol (Engl Ed)* 2016;69:188-200.
  33. Cademartiri F, Seitun S, Clemente A, et al. Myocardial blood flow quantification for evaluation of coronary artery disease by computed tomography. *Cardiovasc Diagn Ther* 2017;7:129-50.
  34. Mehra VC, Valdiviezo C, Arbab-Zadeh A, et al. A stepwise approach to the visual interpretation of CT-based myocardial perfusion. *J Cardiovasc Comput Tomogr* 2011;5:357-69.
  35. Danad I, Fayad ZA, Willemink MJ, et al. New applications of cardiac computed tomography: dual-energy, spectral, and molecular CT imaging. *JACC Cardiovasc Imaging* 2015;8:710-23.

36. Danad I, Szymonifka J, Schulman-Marcus J, et al. Static and dynamic assessment of myocardial perfusion by computed tomography. *Eur Heart J Cardiovasc Imaging* 2016;17:836-44.
37. Rochitte CE, George RT, Chen MY, et al. Computed tomography angiography and perfusion to assess coronary artery stenosis causing perfusion defects by single photon emission computed tomography: the CORE320 study. *Eur Heart J* 2014;35:1120-30.
38. George RT, Mehra VC, Chen MY, et al. Myocardial CT Perfusion Imaging and SPECT for the Diagnosis of Coronary Artery Disease: A Head-to-Head Comparison from the CORE320 Multicenter Diagnostic Performance Study. *Radiology* 2014;272:407-16. Erratum in: *Radiology* 2015;274:626.
39. Magalhães TA, Kishi S, George RT, et al. Combined coronary angiography and myocardial perfusion by computed tomography in the identification of flow-limiting stenosis - The CORE320 study: An integrated analysis of CT coronary angiography and myocardial perfusion. *J Cardiovasc Comput Tomogr* 2015;9:438-45.
40. Cury RC, Kitt TM, Feaheny K, et al. A randomized, multicenter, multivendor study of myocardial perfusion imaging with regadenoson CT perfusion vs single photon emission CT. *J Cardiovasc Comput Tomogr* 2015;9:103-12.e1-2.
41. Fukuda N, Terui T, Ohtsuki I, et al. Titin and troponin: central players in the frank-starling mechanism of the heart. *Curr Cardiol Rev* 2009;5:119-24.
42. Berne RM. Regulation of coronary blood flow. *Physiol Rev* 1964;44:1-29.
43. Krasnow N, Gorlin R. Myocardial lactate metabolism in coronary insufficiency. *Ann Intern Med* 1963;59:781-7.
44. Uren NG, Melin JA, De Bruyne B, et al. Relation between Myocardial Blood Flow and the Severity of Coronary-Artery Stenosis. *N Engl J Med* 1994;330:1782-8.
45. Tonino PA, Fearon WF, De Bruyne B, et al. Angiographic versus functional severity of coronary artery stenoses in the FAME study fractional flow reserve versus angiography in multivessel evaluation. *J Am Coll Cardiol* 2010;55:2816-21.
46. Stillman AE, Oudkerk M, Bluemke DA, et al. Imaging the myocardial ischemic cascade. *Int J Cardiovasc Imaging* 2018;34:1249-63.
47. Picano E, Lattanzi F, Masini M, et al. Usefulness of the dipyridamole-exercise echocardiography test for diagnosis of coronary artery disease. *Am J Cardiol* 1988;62:67-70.
48. Charoenpanichkit C, Hundley WG. The 20 year evolution of dobutamine stress cardiovascular magnetic resonance. *J Cardiovasc Magn Reson* 2010;12:59.
49. Cury RC, Kitt TM, Feaheny K, et al. Regadenoson-stress myocardial CT perfusion and single-photon emission CT: rationale, design, and acquisition methods of a prospective, multicenter, multivendor comparison. *J Cardiovasc Comput Tomogr* 2014;8:2-12.
50. Reyes E. Regadenoson stress for myocardial perfusion imaging. *Future Cardiol* 2016;12:59-67.
51. Topol EJ, Nissen SE. Our preoccupation with coronary luminology: The dissociation between clinical and angiographic findings in ischemic heart disease. *Circulation* 1995;92:2333-42.
52. van de Hoef TP, Meuwissen M, Escaned J, et al. Fractional flow reserve as a surrogate for inducible myocardial ischaemia. *Nat Rev Cardiol* 2013;10:439-52.
53. De Bruyne B, Fearon WF, Pijls NH, et al. Fractional flow reserve-guided PCI for stable coronary artery disease. *N Engl J Med* 2014;371:1208-17.
54. Smits PC, Abdel-Wahab M, Neumann FJ, et al. Fractional flow reserve-guided multivessel angioplasty in myocardial infarction. *N Engl J Med* 2017;377:397-8.
55. Curzen N, Rana O, Nicholas Z, et al. Does routine pressure wire assessment influence management strategy at coronary angiography for diagnosis of chest pain? the ripcord study. *Circ Cardiovasc Interv* 2014;7:248-55.
56. Ahn JM, Park DW, Shin ES, et al. Fractional Flow Reserve and Cardiac Events in Coronary Artery Disease: Data from a Prospective IRIS-FFR Registry (Interventional Cardiology Research Incooperation Society Fractional Flow Reserve). *Circulation* 2017;135:2241-51.
57. Benenati S, De Maria GL, Scarsini R, et al. Invasive "in the cath-lab" assessment of myocardial ischemia in patients with coronary artery disease: When does the gold standard not apply? *Cardiovasc Revasc Med* 2018;19:362-72.
58. Pijls NHJ, Tonino PAL. The crux of maximum hyperemia: The last remaining barrier for routine use of fractional flow reserve. *JACC Cardiovasc Interv* 2011;4:1093-5.
59. Fearon WF, Bornschein B, Tonino PA, et al. Economic evaluation of fractional flow reserve-guided percutaneous coronary intervention in patients with multivessel disease. *Circulation* 2010;122:2545-50.
60. Sen S, Escaned J, Malik IS, et al. Development and validation of a new adenosine-independent index of stenosis severity from coronary wave-intensity analysis: results of the ADVISE (ADenosine Vasodilator Independent Stenosis Evaluation) study. *J Am Coll Cardiol* 2012;59:1392-402.

61. Götberg M, Christiansen EH, Gudmundsdottir IJ, et al. Instantaneous Wave-free Ratio versus Fractional Flow Reserve to Guide PCI. *N Engl J Med* 2017;376:1813-23.
62. Davies JE, Sen S, Dehbi HM, et al. Use of the instantaneous wave-free ratio or fractional flow reserve in PCI. *N Engl J Med* 2017;376:1824-34.
63. Svanerud J, Ahn JM, Jeremias A, et al. Validation of a novel non-hyperaemic index of coronary artery stenosis severity: The Resting Full-cycle Ratio (VALIDATE RFR) study. *EuroIntervention* 2018;14:806-14.
64. Van't Veer M, Pijls NHJ, Hennigan B, et al. Comparison of Different Diastolic Resting Indexes to iFR: Are They All Equal? *J Am Coll Cardiol* 2017;70:3088-96.
65. Lee JM, Choi KH, Park J, et al. Physiological and Clinical Assessment of Resting Physiological Indexes. *Circulation* 2019;139:889-900. Erratum in: *Circulation* 2019;139:e41.
66. Xu B, Tu S, Qiao S, et al. Diagnostic Accuracy of Angiography-Based Quantitative Flow Ratio Measurements for Online Assessment of Coronary Stenosis. *J Am Coll Cardiol* 2017;70:3077-87.
67. Pellicano M, Lavi I, De Bruyne B, et al. Validation Study of Image-Based Fractional Flow Reserve During Coronary Angiography. *Circ Cardiovasc Interv* 2017;10:e005259.
68. Adams DF, Hessel SJ, Judy PF, et al. Computed tomography of the normal and infarcted myocardium. *AJR Am J Roentgenol* 1976;126:786-91.
69. Higgins CB, Siemers PT, Newell JD, et al. Role of iodinated contrast material in the evaluation of myocardial infarction by computerized transmission tomography. *Invest Radiol* 1980;15:S176-82.
70. McCollough CH, Leng S, Yu L, Fletcher JG. Dual- and Multi-Energy CT: Principles, Technical Approaches, and Clinical Applications. *Radiology* 2015;276:637-53.
71. Pelgrim GJ, van Hamersvelt RW, Willemink MJ, et al. Accuracy of iodine quantification using dual energy CT in latest generation dual source and dual layer CT. *Eur Radiol* 2017;27:3904-12.
72. Marini C, Seitun S, Zawaideh C, et al. Comparison of coronary flow reserve estimated by dynamic radionuclide SPECT and multi-detector x-ray CT. *J Nucl Cardiol* 2017;24:1712-21.
73. Ebersberger U, Marcus RP, Schoepf UJ, et al. Dynamic CT myocardial perfusion imaging: performance of 3D semi-automated evaluation software. *Eur Radiol* 2014;24:191-9.
74. Rossi A, Wragg A, Klotz E, et al. Dynamic Computed Tomography Myocardial Perfusion Imaging: Comparison of Clinical Analysis Methods for the Detection of Vessel-Specific Ischemia. *Circ Cardiovasc Imaging* 2017;10:e005505.
75. Ko BS, Cameron JD, Leung M, et al. Combined CT coronary angiography and stress myocardial perfusion imaging for hemodynamically significant stenoses in patients with suspected coronary artery disease: a comparison with fractional flow reserve. *JACC Cardiovasc Imaging* 2012;5:1097-111.
76. George RT, Arbab-Zadeh A, Miller JM, et al. Computed tomography myocardial perfusion imaging with 320-row detector computed tomography accurately detects myocardial ischemia in patients with obstructive coronary artery disease. *Circ Cardiovasc Imaging* 2012;5:333-40.
77. Bettencourt N, Ferreira ND, Leite D, et al. CAD detection in patients with intermediate-high pre-test probability: low-dose CT delayed enhancement detects ischemic myocardial scar with moderate accuracy but does not improve performance of a stress-rest CT perfusion protocol. *JACC Cardiovasc Imaging* 2013;6:1062-71.
78. Wong DT, Ko BS, Cameron JD, et al. Comparison of diagnostic accuracy of combined assessment using adenosine stress computed tomography perfusion + computed tomography angiography with transluminal attenuation gradient + computed tomography angiography against invasive fractional flow reserve. *J Am Coll Cardiol* 2014;63:1904-12.
79. Yang DH, Kim YH, Roh JH, et al. Stress Myocardial Perfusion CT in Patients Suspected of Having Coronary Artery Disease: Visual and Quantitative Analysis-Validation by Using Fractional Flow Reserve. *Radiology* 2015;276:715-23.
80. Meinel FG, De Cecco CN, Schoepf UJ, et al. First-arterial-pass dual-energy CT for assessment of myocardial blood supply: do we need rest, stress, and delayed acquisition? Comparison with SPECT. *Radiology* 2014;270:708-16.
81. Delgado C, Vázquez M, Oca R, et al. Myocardial ischemia evaluation with dual-source computed tomography: comparison with magnetic resonance imaging. *Rev Esp Cardiol (Engl Ed)* 2013;66:864-70.
82. Kim SM, Chang SA, Shin W, et al. Dual-energy CT perfusion during pharmacologic stress for the assessment of myocardial perfusion defects using a second-generation dual-source CT: a comparison with cardiac magnetic resonance imaging. *J Comput Assist Tomogr* 2014;38:44-52.
83. Ko SM, Park JH, Hwang HK, et al. Direct comparison of stress- and rest-dual-energy computed tomography for

- detection of myocardial perfusion defect. *Int J Cardiovasc Imaging* 2014;30 Suppl 1:41-53.
84. Ko SM, Song MG, Chee HK, et al. Diagnostic performance of dual-energy CT stress myocardial perfusion imaging: direct comparison with cardiovascular MRI. *AJR Am J Roentgenol* 2014;203:W605-13.
  85. Bamberg F, Hinkel R, Schwarz F, et al. Accuracy of dynamic computed tomography adenosine stress myocardial perfusion imaging in estimating myocardial blood flow at various degrees of coronary artery stenosis using a porcine animal model. *Invest Radiol* 2012;47:71-7.
  86. Rossi A, Uitterdijk A, Dijkshoorn M, et al. Quantification of myocardial blood flow by adenosine-stress CT perfusion imaging in pigs during various degrees of stenosis correlates well with coronary artery blood flow and fractional flow reserve. *Eur Heart J Cardiovasc Imaging* 2013;14:331-8.
  87. Schwarz F, Hinkel R, Baloch E, et al. Myocardial CT perfusion imaging in a large animal model: comparison of dynamic versus single-phase acquisitions. *JACC Cardiovasc Imaging* 2013;6:1229-38.
  88. Bamberg F, Hinkel R, Marcus RP, et al. Feasibility of dynamic CT-based adenosine stress myocardial perfusion imaging to detect and differentiate ischemic and infarcted myocardium in an large experimental porcine animal model. *Int J Cardiovasc Imaging* 2014;30:803-12.
  89. Pelgrim GJ, Das M, van Tuijl S, et al. Validation of myocardial perfusion quantification by dynamic CT in an ex-vivo porcine heart model. *Int J Cardiovasc Imaging* 2017;33:1821-30.
  90. Ho KT, Chua KC, Klotz E, et al. Stress and rest dynamic myocardial perfusion imaging by evaluation of complete time-attenuation curves with dual-source CT. *JACC Cardiovasc Imaging* 2010;3:811-20.
  91. Wang Y, Qin L, Shi X, et al. Adenosine-stress dynamic myocardial perfusion imaging with second-generation dual-source CT: comparison with conventional catheter coronary angiography and SPECT nuclear myocardial perfusion imaging. *AJR Am J Roentgenol* 2012;198:521-9.
  92. Greif M, von Ziegler F, Bamberg F, et al. CT stress perfusion imaging for detection of haemodynamically relevant coronary stenosis as defined by FFR. *Heart* 2013;99:1004-11.
  93. Huber AM, Leber V, Gramer BM, et al. Myocardium: dynamic versus single-shot CT perfusion imaging. *Radiology* 2013;269:378-86.
  94. Bamberg F, Marcus RP, Becker A, et al. Dynamic myocardial CT perfusion imaging for evaluation of myocardial ischemia as determined by MR imaging. *JACC Cardiovasc Imaging* 2014;7:267-77.
  95. Rossi A, Dharampal A, Wragg A, et al. Diagnostic performance of hyperaemic myocardial blood flow index obtained by dynamic computed tomography: does it predict functionally significant coronary lesions? *Eur Heart J Cardiovasc Imaging* 2014;15:85-94.
  96. Coenen A, Rossi A, Lubbers MM, et al. Integrating CT Myocardial Perfusion and CT-FFR in the Work-Up of Coronary Artery Disease. *JACC Cardiovasc Imaging* 2017;10:760-70.
  97. Yi Y, Xu C, Wu W, et al. Myocardial blood flow analysis of stress dynamic myocardial CT perfusion for hemodynamically significant coronary artery disease diagnosis: The clinical value of relative parameter optimization. *J Cardiovasc Comput Tomogr* 2020;14:314-21.
  98. Rief M, Chen MY, Vavere AL, et al. Coronary Artery Disease: Analysis of Diagnostic Performance of CT Perfusion and MR Perfusion Imaging in Comparison with Quantitative Coronary Angiography and SPECT-Multicenter Prospective Trial. *Radiology* 2018;286:461-70.
  99. Sharma RK, Arbab-Zadeh A, Kishi S, et al. Incremental diagnostic accuracy of computed tomography myocardial perfusion imaging over coronary angiography stratified by pre-test probability of coronary artery disease and severity of coronary artery calcification: The CORE320 study. *Int J Cardiol* 2015;201:570-7.
  100. Bischoff B, Deseive S, Rampp M, et al. Myocardial ischemia detection with single-phase CT perfusion in symptomatic patients using high-pitch helical image acquisition technique. *Int J Cardiovasc Imaging* 2017;33:569-76.
  101. Rief M, Zimmermann E, Stenzel F, et al. Computed tomography angiography and myocardial computed tomography perfusion in patients with coronary stents: prospective intraindividual comparison with conventional coronary angiography. *J Am Coll Cardiol* 2013;62:1476-85.
  102. Takx RA, Blomberg BA, El Aidi H, et al. Diagnostic accuracy of stress myocardial perfusion imaging compared to invasive coronary angiography with fractional flow reserve meta-analysis. *Circ Cardiovasc Imaging* 2015;8:e002666.
  103. Celeng C, Leiner T, Maurovich-Horvat P, et al. Anatomical and Functional Computed Tomography for Diagnosing Hemodynamically Significant Coronary Artery Disease: A Meta-Analysis. *JACC Cardiovasc Imaging* 2019;12:1316-25.
  104. Williams MC, Mirsadraee S, Dweck MR, et al. Computed

- tomography myocardial perfusion vs (15)O-water positron emission tomography and fractional flow reserve. *Eur Radiol* 2017;27:1114-24.
105. Wichmann JL, Meinel FG, Schoepf UJ, et al. Absolute Versus Relative Myocardial Blood Flow by Dynamic CT Myocardial Perfusion Imaging in Patients With Anatomic Coronary Artery Disease. *AJR Am J Roentgenol* 2015;205:W67-72.
  106. Kono AK, Coenen A, Lubbers M, et al. Relative myocardial blood flow by dynamic computed tomographic perfusion imaging predicts hemodynamic significance of coronary stenosis better than absolute blood flow. *Invest Radiol* 2014;49:801-7.
  107. Coenen A, Lubbers MM, Kurata A, et al. Diagnostic value of transmural perfusion ratio derived from dynamic CT-based myocardial perfusion imaging for the detection of haemodynamically relevant coronary artery stenosis. *Eur Radiol* 2017;27:2309-16.
  108. Lu M, Wang S, Sirajuddin A, et al. Dynamic stress computed tomography myocardial perfusion for detecting myocardial ischemia: A systematic review and meta-analysis. *Int J Cardiol* 2018;258:325-31.
  109. Chen MY, Rochitte CE, Arbab-Zadeh A, et al. Prognostic value of combined CT angiography and myocardial perfusion imaging versus invasive coronary angiography and nuclear stress perfusion imaging in the prediction of major adverse cardiovascular events: the CORE320 multicenter study. *Radiology* 2017;284:55-65.
  110. Meinel FG, Pugliese F, Schoepf UJ, et al. Prognostic Value of Stress Dynamic Myocardial Perfusion CT in a Multicenter Population With Known or Suspected Coronary Artery Disease. *AJR Am J Roentgenol* 2017;208:761-9.
  111. Meinel FG, Wichmann JL, Schoepf UJ, et al. Global quantification of left ventricular myocardial perfusion at dynamic CT imaging: Prognostic value. *J Cardiovasc Comput Tomogr* 2017;11:16-24.
  112. Nakamura S, Kitagawa K, Goto Y, et al. Incremental Prognostic Value of Myocardial Blood Flow Quantified With Stress Dynamic Computed Tomography Perfusion Imaging. *JACC Cardiovasc Imaging* 2019;12:1379-87.
  113. van Assen M, De Cecco CN, Eid M, et al. Prognostic value of CT myocardial perfusion imaging and CT-derived fractional flow reserve for major adverse cardiac events in patients with coronary artery disease. *J Cardiovasc Comput Tomogr* 2019;13:26-33.
  114. Song YB, Arbab-Zadeh A, Matheson MB, et al. Contemporary Discrepancies of Stenosis Assessment by Computed Tomography and Invasive Coronary Angiography. *Circ Cardiovasc Imaging* 2019;12:e007720.
  115. Jia CF, Zhong J, Meng XY, et al. Image quality and diagnostic value of ultra low-voltage, ultra low-contrast coronary CT angiography. *Eur Radiol* 2019;29:3678-85.
  116. Fujita M, Kitagawa K, Ito T, et al. Dose reduction in dynamic CT stress myocardial perfusion imaging: comparison of 80-kV/370-mAs and 100-kV/300-mAs protocols. *Eur Radiol* 2014;24:748-55.
  117. Tesche C, De Cecco CN, Albrecht MH, et al. Coronary CT Angiography-derived Fractional Flow Reserve. *Radiology* 2017;285:17-33.
  118. Mastrodicasa D, Albrecht MH, Schoepf UJ, et al. Artificial intelligence machine learning-based coronary CT fractional flow reserve (CT-FFR(ML)): Impact of iterative and filtered back projection reconstruction techniques. *J Cardiovasc Comput Tomogr* 2019;13:331-5.
  119. Siogkas PK, Anagnostopoulos CD, Liga R, et al. Noninvasive CT-based hemodynamic assessment of coronary lesions derived from fast computational analysis: a comparison against fractional flow reserve. *Eur Radiol* 2019;29:2117-26.
  120. National Institute for Health and Care Excellence (NICE) HeartFlow FFRCT for estimating fractional flow reserve from coronary CT angiography. Medical Technologies Guidance 32. February, 2017. Available online: <https://www.nice.org.uk/guidance/mtg32/resources>
  121. Sakellarios AI, Rigas G, Kigka V, et al. SMARTool: A tool for clinical decision support for the management of patients with coronary artery disease based on modeling of atherosclerotic plaque process. *Annu Int Conf IEEE Eng Med Biol Soc* 2017;2017:96-9.
  122. Sakellarios A, Correia J, Kyriakidis S, et al. A cloud-based platform for the non-invasive management of coronary artery disease. *Enterprise Information Systems* 2020. [Epub ahead of print].
  123. Kruk M, Wardziak Ł, Demkow M, et al. Workstation-Based Calculation of CTA-Based FFR for Intermediate Stenosis. *JACC Cardiovasc Imaging* 2016;9:690-9.
  124. Ko BS, Cameron JD, Munnur RK, et al. Noninvasive CT-Derived FFR Based on Structural and Fluid Analysis: A Comparison With Invasive FFR for Detection of Functionally Significant Stenosis. *JACC Cardiovasc Imaging* 2017;10:663-73.
  125. Siogkas PK, Sakellarios AI, Kyriakidis SK, et al. The effect of error propagation in the 3D reconstruction of coronary segments using CTCA images on crucial hemodynamic parameters. *Annu Int Conf IEEE Eng Med Biol Soc*

- 2019;2019:5006-9.
126. Koo BK, Erglis A, Doh JH, et al. Diagnosis of ischemia-causing coronary stenoses by noninvasive fractional flow reserve computed from coronary computed tomographic angiograms. Results from the prospective multicenter DISCOVER-FLOW (Diagnosis of Ischemia-Causing Stenoses Obtained Via Noninvasive Fractional Flow Reserve) study. *J Am Coll Cardiol* 2011;58:1989-97.
  127. Min JK, Leipsic J, Pencina MJ, et al. Diagnostic accuracy of fractional flow reserve from anatomic CT angiography. *JAMA* 2012;308:1237-45.
  128. Nørgaard BL, Leipsic J, Gaur S, et al. Diagnostic performance of noninvasive fractional flow reserve derived from coronary computed tomography angiography in suspected coronary artery disease: the NXT trial (Analysis of Coronary Blood Flow Using CT Angiography: Next Steps). *J Am Coll Cardiol* 2014;63:1145-55.
  129. Douglas PS, De Bruyne B, Pontone G, et al. 1-Year Outcomes of FFRCT-Guided Care in Patients With Suspected Coronary Disease: The PLATFORM Study. *J Am Coll Cardiol* 2016;68:435-45.
  130. Lu MT, Ferencik M, Roberts RS, et al. Noninvasive FFR Derived From Coronary CT Angiography: Management and Outcomes in the PROMISE Trial. *JACC Cardiovasc Imaging* 2017;10:1350-8.
  131. Kim KH, Doh JH, Koo BK, et al. A novel noninvasive technology for treatment planning using virtual coronary stenting and computed tomography-derived computed fractional flow reserve. *JACC Cardiovasc Interv* 2014;7:72-8.
  132. Renker M, Schoepf UJ, Wang R, et al. Comparison of diagnostic value of a novel noninvasive coronary computed tomography angiography method versus standard coronary angiography for assessing fractional flow reserve. *Am J Cardiol* 2014;114:1303-8.
  133. Coenen A, Lubbers MM, Kurata A, et al. Fractional flow reserve computed from noninvasive CT angiography data: diagnostic performance of an on-site clinician-operated computational fluid dynamics algorithm. *Radiology* 2015;274:674-83.
  134. Cook CM, Petraco R, Shun-Shin MJ, et al. Diagnostic Accuracy of Computed Tomography-Derived Fractional Flow Reserve: A Systematic Review. *JAMA Cardiol* 2017;2:803-10. Erratum in: *JAMA Cardiol* 2017;2:1284.
  135. Rosa GM, Bauckneht M, Masoero G, et al. The vulnerable coronary plaque: update on imaging technologies. *Thromb Haemost* 2013;110:706-22.
  136. Driessen RS, Stuijzand WJ, Raijmakers PG, et al. Effect of Plaque Burden and Morphology on Myocardial Blood Flow and Fractional Flow Reserve. *J Am Coll Cardiol* 2018;71:499-509.
  137. Gaur S, Øvrehus KA, Dey D, et al. Coronary plaque quantification and fractional flow reserve by coronary computed tomography angiography identify ischaemia-causing lesions. *Eur Heart J* 2016;37:1220-7.
  138. Ahmadi A, Kini A, Narula J. Discordance between ischemia and stenosis, or PINSS and NIPSS: are we ready for new vocabulary? *JACC Cardiovasc Imaging* 2015;8:111-4.
  139. Ferencik M, Lu MT, Mayrhofer T, et al. Non-invasive fractional flow reserve derived from coronary computed tomography angiography in patients with acute chest pain: Subgroup analysis of the ROMICAT II trial. *J Cardiovasc Comput Tomogr* 2019;13:196-202.
  140. Kawaji T, Shiomi H, Morishita H, et al. Feasibility and diagnostic performance of fractional flow reserve measurement derived from coronary computed tomography angiography in real clinical practice. *Int J Cardiovasc Imaging* 2017;33:271-81.
  141. Rabbat M, Leipsic J, Bax J, et al. Fractional Flow Reserve Derived from Coronary Computed Tomography Angiography Safely Defers Invasive Coronary Angiography in Patients with Stable Coronary Artery Disease. *J Clin Med* 2020;9:604.

**Cite this article as:** Seitun S, Clemente A, De Lorenzi C, Benenati S, Chiappino D, Mantini C, Sakellarios AI, Cademartiri F, Bezante GP, Porto I. Cardiac CT perfusion and FFR<sub>CTA</sub>: pathophysiological features in ischemic heart disease. *Cardiovasc Diagn Ther* 2020;10(6):1954-1978. doi: 10.21037/cdt-20-414